

12 57
11 1980

12

DTIC ELECTED
OCT 2 1980

6

Ocean Tides, Part I Global Ocean Tidal Equations,

10 Ernst W/Schwiderski

U. S. Naval Surface Weapons Center
Dahlgren, Virginia

AD A089899

A detailed derivation of improved ocean tidal equations in continuous (COTEs) and discrete (DOTEs) forms is presented. These equations feature the Boussinesq linear eddy dissipation law with a novel eddy viscosity that depends on the lateral mesh area, i.e., on mesh size and ocean depth. Analogously, the linear law of bottom friction is used with a new bottom friction coefficient depending on the bottom mesh area. The primary astronomical tide-generating potential is modified by secondary effects due to the oceanic and terrestrial tides. The fully linearized equations are defined in a single-layer ocean basin of realistic bathymetry varying from 50 m to 7,000 m. The DOTEs are set up on a 1° by 1° spherically graded grid system, using central finite differences in connection with Richardson's staggered computation scheme. Mixed single-step finite differences in time are introduced, which enhance decay, dispersion, and stability properties of the DOTEs and facilitate—in Part II of this paper—a unique hydrodynamical interpolation of empirical tide data. The purely hydrodynamical modeling is completed by imposing boundary conditions consisting of no-flow across and free-slip along the mathematical ocean shorelines. Shortcomings of the constructed preliminary M₂ ocean tide charts are briefly discussed. Needed improvements of the model are left to Part II.

DDC FILE COPY.

Marine Geodesy, Volume 3
0149-0419/80/0131-0161 \$02.00/0
Copyright © 1980, Crane, Russak & Co., Inc.

411567

JOB

80 9 26 020

bulent motions of a viscous, incompressible fluid including all unknown Reynolds stresses (see, e.g., Schlichting, 1968), which must provide the major friction stress to keep the intrinsic supercritical instability of the flow under control. In rotating spherical polar coordinates (λ, ϕ, r) , these equations may be written in the form (see, e.g., Whitaker, 1968):

$$\begin{aligned}
 u_r + \frac{u}{r \cos \phi} u_\lambda + \frac{v}{r} u_\phi + w u_r - \frac{uv}{r} - \frac{uv}{r} \tan \phi + \frac{uw}{r} \\
 = \frac{1}{r \cos \phi} \left(q - \frac{p}{\rho} \right)_\lambda + 2\Omega(v \sin \phi - w \cos \phi) + f^\lambda, \quad (1a)
 \end{aligned}$$

$$\begin{aligned}
 v_r = \frac{u}{r \cos \phi} v_\lambda + \frac{v}{r} v_\phi + w v_r + \frac{u^2}{r} \tan \phi + \frac{vw}{r} \\
 = \frac{1}{r} \left(q - \frac{p}{\rho} \right)_\phi - 2\Omega u \sin \phi - \frac{1}{2} \Omega^2 r \sin 2\phi + f^\phi, \quad (1b)
 \end{aligned}$$

$$\begin{aligned}
 w_r + \frac{u}{r \cos \phi} w_\lambda + \frac{v}{r} w_\phi + w w_r - \frac{1}{r} (u^2 + v^2) \\
 = - \left(G + \frac{1}{\rho} \mu_r \right) + 2\Omega u \cos \phi + \Omega^2 r \cos^2 \phi + f^r, \quad (1c)
 \end{aligned}$$

$$\frac{1}{r \cos \phi} [u_\lambda + (v \cos \phi)_\phi] + \frac{1}{r^2} (r^2 w)_r = 0, \quad (2)$$

$$\rho f^\lambda = \frac{1}{r \cos \phi} \tau_\lambda^{\lambda\lambda} + \frac{1}{r} \tau_\phi^{\lambda\phi} + \tau_r^{\lambda r} + \frac{3}{r} \tau^{\lambda r} - \frac{2}{r} \tau^{\lambda\phi} \tan \phi, \quad (3a)$$

$$\begin{aligned}
 \rho f^\phi = \frac{1}{r \cos \phi} [\tau_\lambda^{\lambda\phi} + (\tau^{\phi\phi} \cos \phi)_\phi] + \tau^{\phi r} \\
 + \frac{3}{r} \tau^{\phi r} + \frac{1}{r} \tau^{\lambda\lambda} \tan \phi, \quad (3b)
 \end{aligned}$$

$$\begin{aligned}
 \rho f^r = \frac{1}{r \cos \phi} [\tau_\lambda^{\lambda r} + (\tau^{\phi r} \cos \phi)_\phi] + \tau_r^{rr} \\
 + \frac{1}{r} (2\tau^{rr} - \tau^{\phi\phi} - \tau^{\lambda\lambda}), \quad (3c)
 \end{aligned}$$

In these equations, all subscripts denote indicated partial derivatives, while all superscripts denote indicated components of the turbulent dissipation vector f or the Reynolds stress tensor τ . Furthermore, the following notations are used:

t	= universal time in sec
λ	= east longitude
ϕ	= $\frac{\pi}{2} - \theta$ = north latitude (θ = colatitude)
r	= polar radius in m
(u, v, w)	= east, north, and radial velocities, respectively, in m/sec (averaged)
p	= pressure (averaged)
q	= total tide-generating potential
f	= dissipation vector
τ	= Reynolds stress tensor (to be specified)
Ω	= $0.72722 \times 10^{-4} \text{ sec}^{-1}$ = earth angular velocity
ρ	$\approx 10^3 \text{ kg/m}^3$ = density of sea water
G	= 9.81 m/sec^2 = gravity acceleration

The equations of turbulent "mean" motion are obtained by a formal time-averaging procedure applied to the Navier-Stokes equations of viscous laminar flow that leads to the concepts of "averaged" velocities and pressure, as well as to the unknown Reynolds stress tensor, τ , containing the filtered out, fluctuating velocity residuals in quadratic form (see, e.g., Schlichting, 1968). A discussion of the physical meaning of these and following turbulence motions may be postponed to the section, "Discrete Versus Continuous Ocean-Tide Equations." The momentum equations (Equations 1) maintain the momentum balance between the familiar kinetic forces on the left side and the forces of potential (tide, gravity, and pressure), Coriolis, centrifugal acceleration, and dissipation on the right side. The continuity equation (Equation 2) expresses the condition of conservation of incompressible mass. The Reynolds stress tensor, τ , and the total tide-generating potential, q , will be specified in the next two sections. The global oceans at hydrostatic rest may be described by the following surface and bottom boundary conditions:

- (1) $r = R = 0.637 \times 10^7 \text{ m}$ = spherical (geoidal rest) sea surface (all geoidal undulations are neglected without any significant loss of accuracy),
- (2) $r = R - H(\lambda, \phi)$ = sea-bottom relief, where
- (3) $H = H(\lambda, \phi)$ = realistic ocean depth in m $H(\lambda, \phi) = 0$ for land points, see section "The 1° by 1° Graded Grid System and Bathymetry," and
- (4) $p = P - G\rho z$ = hydrostatic sea-pressure distribution with constant (arbitrary) sea-surface pressure P , where
- (5) $z = r - R$ = new depth variable, so that $z = 0$ denotes $r = R$ (see Figure 1).

Due to the time-dependent, tide-generating potential, q , acting on the ocean and solid earth, the hydrostatic conditions (1)–(5) are altered to the following hydrodynamical boundary values (see Figure 1):

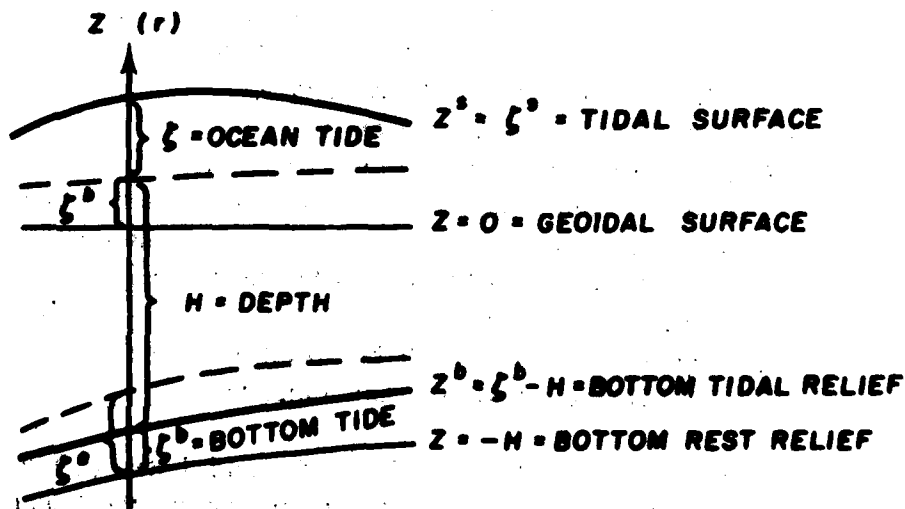


Figure 1. Earth-ocean tidal interaction: ζ = ocean tide, ζ^e = earth tide, ζ^s = surface tide, ζ^b = bottom tide, $\zeta^o = \zeta^e - \zeta^b$ = earth dip-response to ocean tide, and H = ocean depth.

- (a) $z^s = \zeta^s = \zeta^s(\lambda, \phi, t)$ = total sea-surface tidal elevation over geoid $z = 0$;
- (b) $z^b = \zeta^b(\lambda, \phi, t) - H(\lambda, \phi)$ = sea-bottom tidal relief, where
- (c) $\zeta^b = \zeta^b(\lambda, \phi, t)$ = total bottom tidal elevation over rest relief $z = -H(\lambda, \phi)$;
- (d) $\zeta = \zeta(\lambda, \phi, t) = \zeta^s - \zeta^b$ = ocean tidal elevation (measured by bottom tidal pressure gauges) to be modeled;
- (e) $\zeta^e = \zeta^e(\lambda, \phi, t)$ = earth tidal elevation to be specified (Equations 9);
- (f) $\zeta^{eo} = \zeta^{eo}(\lambda, \phi, t) = \zeta^e - \zeta^b$ = earth dip-response to oceanic tidal load, ζ (Equation 10);
- (g) $p^s = P$ = constant surface pressure (no atmospheric pressure considered);
- (h) $w^s = \zeta_s^s$ = surface radial velocity;
- (i) $\tau^s = 0$ = no surface stress (free-slip, no wind force considered);
- (j) $(u^b, v^b, w^b) \cdot \nabla(H + z) = \tau_z^b = 0$ = no flow across ocean bottom (∇ = gradient vector);
- (k) $\tau^b = \rho B(u^b, v^b)$ = bottom stress vector specified by invoking the linear law of bottom friction with the coefficient
- $$B = b\mu \cos \phi = \bar{b}L^2 \mu \cos \phi \quad (4a)$$
- depending on the cell bottom area $L^2 \mu \cos \phi$, where
- (l) L = chosen equatorial mesh size (section "The $1^\circ \times 1^\circ$ Graded Grid System and Bathymetry"),
- (m) μ = mesh "grading" parameter (section "The $1^\circ \times 1^\circ$ Graded Grid System and Bathymetry"), and
- (n) $b = \bar{b}L^2$ = uniform bottom friction parameter, which must be determined by trial-and-error computations for best results. The final M_2 tide (Schwiderski, 1979b) was computed with $b = 0.01$ m/sec. (4b)
- (o) Lateral boundary data will be specified in the section, "Lateral-Boundary, Initial, and Final Data."

In contrast to Zehel (1970, 1973, 1975) and Estes (1975, 1977), who used the nonlinear law of bottom friction, the linear law is here preferred as it is more consistent with the overall Stokes

slow-motion assumptions (see, e.g., Schlichting, 1968) characterizing the present tide model (section, "The Continuous Ocean-Tide Equations (COTEs).") Especially the computations by Estes (1975, Figure 6) indicate no need for any nonlinear friction terms, at least not in deep ocean areas. Pekeris and Accad (1969) used the same linear law of bottom friction and called attention to earlier work by Grace (1931) in the Gulf of Suez. Grace applied both laws and experienced a slight preference for the linear law.

In deviation from Pekeris and Accad, the present bottom friction coefficient is assumed independent of ocean depth. Since those authors placed their artificial boundaries of the world oceans at the 1,000-m depth level, it was plausible to restrict any significant bottom friction to those boundaries. This was accomplished by simply assuming a bottom friction coefficient B that depended inversely on the ocean depth. In the present tide model, which uses (section, "The $1^\circ \times 1^\circ$ Graded Grid System and Bathymetry"), a bathymetry that varies from 50 m to 7,000 m (or 10 m to 7,000 m in Schwiderski, 1979b), this assumption was found unjustified. Bottom friction coefficients of the form $B \sim H^e$ have been tested for $e = -1$ (Pekeris and Accad assumption), $e = -\frac{1}{2}$, and $e = 0$. The latter case appeared to yield best results.

The assumed dependence of the bottom friction coefficient B on the bottom mesh-cell area (Equation 4a) is in agreement with the novel law of eddy viscosity, which is introduced below in the next section and which is further discussed in the section, "Discrete Versus Continuous Ocean-Tide Equations." In fact, as can be seen from Equations 28, the bottom friction coefficient is essentially determined by the vertical eddy viscosity. It may be noted that the numerical values of the bottom friction coefficient (Equations 4a and b) used in the present model fall considerably below those used by Pekeris and Accad in their corresponding domains, where friction is essentially restricted to the boundary line.

Reynolds Stresses and Eddy Dissipation

The formally derived unknown Reynolds stress tensor, τ (preceding section), may be specified by the original Boussinesq (1877)

substitution (see section, "The $1^\circ \times 1^\circ$ Graded Grid System and Bathymetry"); that is, by the laminar, viscous stress tensor (see, e.g., Schlichting, 1968; Whitaker, 1968):

$$\tau^{\lambda\lambda} = 2\rho A \left[\frac{1}{r \cos \phi} u_\lambda - \frac{v}{r} \tan \phi + \frac{w}{r} \right], \quad (5a)$$

$$\tau^{\phi\phi} = 2\rho A \left[\frac{1}{r} v_\phi + \frac{w}{r} \right], \quad (5b)$$

$$\tau^{rr} = 2\rho A w_r, \quad (5c)$$

$$\tau^{\lambda\lambda} = \tau^{\phi\lambda} = \rho A \left[\frac{\cos \phi}{r} \left(\frac{u}{\cos \phi} \right)_\phi + \frac{1}{r \cos \phi} v_\lambda \right], \quad (5d)$$

$$\tau^{\lambda r} = \tau^{r\lambda} = \rho A \left[r \left(\frac{u}{r} \right)_r + \frac{1}{r \cos \phi} w_\lambda \right], \quad (5e)$$

$$\tau^{\phi r} = \tau^{r\phi} = \rho A \left[\left(\frac{v}{r} \right)_r + \frac{1}{r} w_\phi \right]. \quad (5f)$$

In this substitution, the ordinary kinetic molecular viscosity is replaced by the so-called "eddy viscosity" A (momentum Austausch, exchange, or mixing coefficient), which remains to be modeled to represent the true turbulent flow characteristics at hand as closely as possible.

In order to achieve a greater modeling flexibility, it is customary to divide the eddy viscosity into a "vertical" eddy viscosity associated with vertical shear and into a "horizontal" (lateral) eddy viscosity associated with horizontal shear. Since east and north dimensions are usually nearly equal, no need for two lateral eddy viscosities has ever been encountered. In single-layer ocean models like the present one (section, "The Continuous Ocean-Tide Equations (COTEs)," the separate treatment of the vertical eddy viscosity needs no explicit specification, because (Equations 28) the viscosity becomes an important part of the bottom-friction coefficient, B , defined by Equations 4a and 4b.

Based on the author's extensive computer experiments and on the physical arguments elaborated on in the sections, "Stability

Analysis" and "Discrete Versus Continuous Ocean-Tide Equations," the (horizontal) eddy viscosity, A , may now be specified by

$$A = \frac{a}{2} LH(\lambda, \phi)(1 + \mu \cos \phi). \quad (6a)$$

In this definition, L and μ denote the mesh size and grading parameters introduced in the preceding section (1,m). Accordingly, the new eddy viscosity depends on the mean lateral cross-section area $H \times L(1 + \mu \cos \phi)/2$ of the flow cell of depth H and average north-east mesh size $L(1 + \mu \cos \phi)/2$. The remaining reduced eddy-dissipation coefficient, a (in sec), must be subjected to trial-and-error computations in order to achieve best results uniformly over all oceans. (Different a -values for the Pacific, North and South Atlantic, and Indian oceans were also tested without significant effects.)

At this point, it may be mentioned that, following Zahel (1970, 1973), the author used in an exploratory tide model a constant eddy viscosity uniformly over all oceans. The results were rather disappointing, especially for shallow ocean-shelf areas, where intolerably low tidal amplitudes were computed. Subsequent computer experiments with eddy viscosities of the form $A \sim H^e$ with $e = 0, 1/2, 1, \text{ and } 3/2$ indicated best results for $e = 1$, as in Equation (6a). Some dependence of the eddy viscosity on the mesh size considered was earlier noticed by Cox (1970), Friedrich (1970), Holland and Hirschman (1972), and Zahel (1975). Indeed, eddy viscosities ranging from $A = 10$ to 10^{11} cm²/sec have been reported as required by many researchers investigating different problems. Obviously, those huge variations of the eddy viscosity can be explained by Equation (6a) by the strong variations of the mesh size L and the depth H considered by different analysts. In the present case with H varying from 10 m to 7,000 m (section, "The 1°×1° Graded Grid System and Bathymetry") the eddy viscosity was found to vary between (section, "Stability Analysis")

$$1.3 \cdot 10^8 \frac{\text{m}^2}{\text{sec}} < A < 1.3 \cdot 10^{10} \frac{\text{m}^2}{\text{sec}}, \quad (6b)$$

which fits the customary range very well. It is perhaps fortuitous, yet interesting, to note that for a cubic cell of about 1-in. mesh size the eddy viscosity, A (Equations 6a, b), reduces to the value of the molecular viscosity of water.

The Total Tide-Generating Potential

The total tide-producing potential, q (section, "The Navier-Stokes Equations of Averaged Turbulent Flow"), may be expressed in the form

$$q = G(\eta + \eta'), \quad (7)$$

where $G\eta$ is the "primary" astronomical potential directly proportional to Newton's equilibrium tide η . The remaining "secondary" potential $G\eta'$ can be expanded into its three major parts

$$G\eta' = G(\eta^o + \eta^e - \eta^{oo}), \quad (8)$$

which reveal their corresponding origins (Figure 1, section, "The Navier-Stokes Equations of Averaged Turbulent Flow" (d), (e), (f)), respectively:

$G\eta^o$ = gravity potential perturbation due to the ocean tide ζ ,
 $G\eta^e$ = gravity potential perturbation due to the earth tide ζ^e ,
 $G\eta^{oo}$ = gravity potential perturbation due to the earth dip-response ζ^{oo} caused by the ocean load (ζ -tide).

Attention to the significance of the earth-ocean tidal interactions manifested in the five quantities ζ^e , η^o , ζ^{oo} , η^{oo} , and η^o was called for by Farrell (1972a, b; 1973). In ocean-tide models, it is sufficient to use the following approximate relations:

$$\zeta^e \sim 0.61\eta, \quad \eta^e \sim 0.30\eta, \quad (9a)$$

$$\zeta^e - \eta^e \sim 0.31\eta, \quad (9b)$$

and

$$\zeta^{oo} - \eta^{oo} + \eta^o \sim 0.10\zeta \quad (10)$$

The first relations (Equations 9) used by Hendershott (1972, 1975), Zahel (1975), Estes (1977), and others, can be justified by second-order Love number approximations. The second relation (Equation 10) has been suggested by Pekeris (presentation given in 1977 at the U.S. Office of Naval Research), who also recommended the factor 0.10 after evaluating the Green's function representation of the three oceanic tidal load effects (ζ^{∞} , η^{∞} , η°) derived by Farrell. Apparently, the suggestion by Pekeris (Equation 10) is physically just as plausible as the accepted approximation (Equations 9). In Equations 9a and b, it is assumed that the solid-earth tide, ζ^e , and its subsequent gravity perturbation, $G\eta^e$, are essentially instantaneous responses to the tide-generating potential, q . Analogously, in Equation 10, it is assumed that the solid-earth dip, ζ^{∞} , and the gravity perturbations, η^{∞} and η° , are almost instantaneous responses to the ocean's tidal load, ζ . It may be mentioned that the author conducted extensive computer experiments using the factors 0.00, 0.08, and 0.12 instead of 0.10 in Equation 10. The last two factors produced no noteworthy alterations of the results. The first factor (0.00) obviously deletes all oceanic tidal-load effects to which critically large significance has been attached by Hendershott (1972, 1975). The author's computations supported the marginal effects of oceanic tidal loading found by Estes (1977).

Following Thomson (1868), Darwin (1883), Doodson (1921), and Cartwright and Taylor (1971), the primary astronomical tide-generating potential, $G\eta$, or, equivalently, the equilibrium tide, η , may be expanded into a series (see, e.g., Dietrich, 1963) of "harmonic components" (constituents), η_v , with a nonharmonic frequency spectrum

$$\eta = \sum_{v=0}^{\infty} \eta_v(\lambda, \phi, t). \quad (11)$$

In the final analysis of ocean tides, the following three major species will have to be considered:

(a) Semidiurnal Equilibrium Tides

$$v = 2: \eta_2 = K \cos^2 \phi \cos(\sigma t + 2\lambda + \chi) \quad (12)$$

(b) Diurnal Equilibrium Tides

$$v = 1: \eta_1 = K \sin 2\phi \cos(\sigma t + \lambda + \chi) \quad (13)$$

(c) Long-Period Equilibrium Tides

$$v = 0: \eta_0 = K(3 \cos^2 \phi - 2) \cos(\sigma t + \chi) \quad (14)$$

In Equations 12-14, the constants (K, σ, χ) denote K = amplitude of equilibrium tide (in m), σ = frequency of equilibrium tide (in sec^{-1}), χ = astronomical argument of equilibrium tide (in rad).

In Table 1, these constants are listed for the major tidal modes

Table 1
Constants of major tidal modes.

Tidal Mode	$K^a(m)$	$\sigma^b(10^{-4}/\text{sec})$	$\chi^c(\text{deg})$
<i>Semidiurnal Species</i>			
M_2 = Principal Lunar	0.242 334	1.405 19	$2h_0^d - 2s_0$
S_2 = Principal Solar	0.112 841	1.454 44	0
N_2 = Elliptical Lunar	0.046 398	1.378 80	$2h_0 - 3s_0 + p_0$
K_2 = Declination Luni-Solar	0.030 704	1.458 42	$2h_0$
<i>Diurnal Species</i>			
K_1 = Declination Luni-Solar	0.141 565	0.729 21	$h_0 + 90$
O_1 = Principal Lunar	0.100 514	0.675 98	$h_0 - 2s_0 - 90$
P_1 = Principal Solar	0.046 843	0.725 23	$-h_0 - 90$
Q_1 = Elliptical Lunar	0.019 256	0.649 59	$h_0 - 2s_0 + p_0 - 90$
<i>Long-Period Species</i>			
M_f = Fortnightly Lunar	0.041 742	0.053 234	$2s_0$
M_m = Monthly Lunar	0.022 026	0.026 392	$s_0 - p_0$
S_{sa} = Semiannual Solar	0.019 446	0.003 982	$2h_0$

^a K = amplitude of the partial tide.

^b σ = frequency of the partial tide.

^c χ = astronomical argument of the partial tide.

^d (h_0, s_0, p_0) = mean longitudes of sun, moon, and lunar perigee at Greenwich midnight;

$$h_0 = 279.696\ 68 + 36\ 000.768\ 930\ 485\ T + 3.03 \cdot 10^{-4}T^2,$$

$$s_0 = 270.434\ 358 + 481\ 267.883\ 141\ 37T - 0.001\ 133T^2 + 1.9 \cdot 10^{-6}T^3,$$

$$p_0 = 334.329\ 653 + 4\ 069.034\ 032\ 957\ 5T - 0.010\ 325T^2 - 1.2 \cdot 10^{-5}T^3,$$

where

$$T = [27\ 392.500\ 528 + 1.000\ 000\ 035\ 6D]/36\ 525,$$

$$D = d + 365(y - 1975) + \text{Int}[(y - 1975)/4],$$

d = day number of year ($d = 1$ for January 1),

$y \geq 1975$ = year number,

and

$\text{Int}[x]$ = integral part of x .

with amplitudes larger than 4% of the leading semidiurnal moon (M_2) tide. The daily astronomical argument, χ , can be neglected in the following construction of the oceanic tidal modes

$$\zeta = \xi(\lambda, \phi) \cos(\sigma t + \chi - \delta(\lambda, \phi)) \quad (15a)$$

corresponding to the considered mode of the equilibrium tide, $\eta = \eta_0$. According to Equation 15a, only the "harmonic constants"

and

$$\left. \begin{aligned} \xi &= \xi(\lambda, \phi) = \text{tidal amplitude (in m)} \\ \delta &= \delta(\lambda, \phi) = \text{Greenwich phase (in rad)} \end{aligned} \right\} (15b)$$

need to be found, provided the tide model is linear or almost linear.

The Continuous Ocean-Tide Equations (COTEs)

In addition to the simplifying assumptions made in the three preceding sections concerning bottom friction ((k)-(n)), eddy dissipation, and total tide-generating potential, the following simplifications may be invoked:

- (a) Hydrostatic pressure assumption in Equations 1; i.e.,
 - (1) Neglect all quadratic inertial accelerations (Stokes' slow-motion assumption consistent with linear eddy dissipation and bottom friction; see, e.g., Schlichting, 1968)
 - (2) Neglect all centrifugal accelerations
 - (3) Neglect vertical Coriolis force
 - (4) Neglect vertical dissipation
 - (5) Neglect vertical motion
- (b) Single-layer ocean assumption in Equations 1 and 2; i.e..
 - (1) $r = R + z \approx R$, but $\partial r = \partial z$
 - (2) $\zeta(\lambda, \phi, t) \ll H(\lambda, \phi)$
 $\zeta^2(\lambda, \phi, t) \ll H(\lambda, \phi)$
 - (3) $u(\lambda, \phi; z, t) \approx u(\lambda, \phi, t)$
 $v(\lambda, \phi; z, t) \approx v(\lambda, \phi, t)$

It may be pointed out that all assumptions of (a) and (b) are well justified over most flow areas. In particular, the strong assumptions (b, 3) are realistic because the tide-generating potential is a body force. Moreover, the motion is fully turbulent and, hence, the averaged velocity profile exhibits only a very thin boundary layer and laminar sublayer (see, e.g., Schlichting, 1968). It may be mentioned that for the same reason the condition of free-slip at a boundary wall (section, "Lateral-Boundary, Initial, and Final Data") seems more appropriate than the no-slip condition used in laminar-flow situations. The assumption (b, 3) is, of course, much less realistic in general ocean currents, which are driven by surface pressure and wind forces and/or by density variations confined to the upper ocean layers.

By applying assumption (a) to Equation 1c, one finds the hydrostatic pressure

$$p_s = -G\rho,$$

i.e.,

$$p - p^* = \int_{z^*}^{\zeta^*} G\rho dz = G\rho(\zeta^* - z),$$

or, with (section, "The Navier-Stokes Equations of Averaged Turbulent Flow" (a)-(g))

$$p^* = P,$$

$$\zeta^* = \zeta + \zeta^0 = \zeta + \zeta^* - \zeta^{**},$$

$$p = G\rho(\zeta + \zeta^* - \zeta^{**} - z) + P.$$

(16)

With Equations 7-10 and 16, one has

$$q - \frac{p}{\rho} = G[\eta - (\zeta^* - \eta^*) - \zeta + (\zeta^{**} - \eta^{**} + \eta^*)] - P/\rho.$$

i.e.,

$$q - \frac{p}{\rho} = G(\alpha\eta - \beta\zeta) - P/\rho. \quad (17a)$$

where

$$\left. \begin{aligned} \alpha &= 0.69, \\ \beta &= 0.90. \end{aligned} \right\} \quad (17b)$$

In the following equations, it is convenient to introduce the notations

$$H_\lambda = H_\lambda/H, \quad H_{\lambda\lambda} = H_{\lambda\lambda}/H, \quad (18)$$

$$H_\phi = H_\phi/H, \quad H_{\phi\phi} = H_{\phi\phi}/H, \quad (19)$$

and

$$\tilde{H}_\phi = H_\phi - \mu \sin\phi / (1 + \mu \cos\phi) \quad (20)$$

so that (Equation 6a)

$$A = AH, \quad A = AH. \quad (21)$$

Using the simplifications (a) and (b) and Equations 17-21 in Equations 1 and 2, one arrives at the reduced equations of motion:

$$u_z = \frac{G}{R \cos\phi} (\alpha\eta - \beta\zeta)_\lambda + 2\Omega v \sin\phi + f^\lambda,$$

$$v_z = \frac{G}{R} (\alpha\eta - \beta\zeta)_\phi - 2\Omega u \sin\phi + f^\phi, \quad (22a)$$

and

$$u + (v \cos\phi)_\phi + R \cos\phi w_z = 0. \quad (23)$$

where (Equations 3a, b; 5a-f; and 21)

$$\begin{aligned}
 f^\lambda &= \frac{A}{R^2 \cos^2 \phi} [u_{\lambda\lambda} + 2\tilde{H}_\lambda u_\lambda - u] + A u_m \\
 &+ \frac{A}{R^2} [u_{\phi\phi} + (\tilde{H}_\phi - \tan \phi) u_\phi + \tilde{H}_\phi u \tan \phi] \\
 &+ \frac{A}{R^2 \cos \phi} [(H_\phi - 2 \tan \phi) v_\lambda - 2\tilde{H}_\lambda v \tan \phi], \quad (24a)
 \end{aligned}$$

$$\begin{aligned}
 f^\phi &= \frac{A}{R^2 \cos \phi} [v_{\lambda\lambda} + \tilde{H}_\lambda v_\lambda - v] + A v_m \\
 &+ \frac{A}{R^2} [v_{\phi\phi} + (2\tilde{H}_\phi - \tan \phi) v_\phi] \\
 &+ \frac{A}{R^2 \cos \phi} [(2u_\lambda + \tilde{H}_\lambda u) \tan \phi + \tilde{H}_\lambda u_\phi]. \quad (24b)
 \end{aligned}$$

Under the single-layer ocean assumption (b), the reduced Equations 22 and 23 may be integrated over the instantaneous ocean depth ($z^a - z^b = H + \zeta$) while observing the surface and bottom boundary data specified in the section, "The Navier-Stokes Equations of Averaged Turbulent Flow." For that purpose, it is useful to introduce the "integrated" velocity components:

$$U(\lambda, \phi, t) = \int_{z^b}^{z^a} u dz \sim uH = (\text{integrated}) \text{ east velocity} \quad (25a)$$

and

$$V(\lambda, \phi, t) = \int_{z^b}^{z^a} v dz \sim vH = (\text{integrated}) \text{ north velocity}, \quad (25b)$$

where the term "integrated" may be omitted when no confusion appears possible.

Using the simplifications and notations made, one finds the helpful approximations with the corresponding replacements ($u \rightarrow v$, $U \rightarrow V$, $\lambda \rightarrow \phi$):

$$\int_{z_0}^{z_1} u_i dz = U_i - u^* z_1^i + u^* z_0^i \sim U_i, \quad (26a)$$

$$\int_{z_0}^{z_1} u_\lambda dz = U_\lambda - u^* z_1^\lambda + u^* z_0^\lambda \sim U_\lambda - H_\lambda U, \quad (26b)$$

and

$$\int_{z_0}^{z_1} u_{\lambda\lambda} dz \sim U_{\lambda\lambda} - H_\lambda U_\lambda + (H_\lambda^2 - H_{\lambda\lambda})U - H_\lambda u_\lambda^*. \quad (26c)$$

The bottom-boundary conditions imposed in the section, "The Navier-Stokes Equations of Averaged Turbulent Flow," (j) and (k) assume the following approximate forms:

$$\zeta_i^b = \frac{H_\lambda}{R \cos \phi} u^b + \frac{H_\phi}{R} v^b + w^b, \quad (27)$$

$$\frac{1}{\rho} \tau^{b\lambda} = \frac{B}{H} U \sim A \left(\frac{H_\lambda u_\lambda^b}{R^2 \cos^2 \phi} + \frac{H_\phi u_\phi^b}{R^2} + u_s^b \right), \quad (28a)$$

and

$$\frac{1}{\rho} \tau^{b\phi} = \frac{B}{H} V \sim A \left(\frac{H_\lambda v_\lambda^b}{R^2 \cos^2 \phi} + \frac{H_\phi v_\phi^b}{R^2} + v_s^b \right). \quad (28b)$$

With Equations 25-28 and the surface-boundary conditions in the section, "The Navier-Stokes Equations of Averaged Turbulent Flow" (h) and (i), the proposed integration of Equations 22 and 23 is easily carried out and yields the following "continuous ocean tidal equations" (COTEs with $\Theta = \pi/2 - \phi =$ colatitude):

$$\begin{aligned} U_i = & \frac{GH}{R \sin \Theta} (\alpha\eta - \beta\zeta)_\lambda - U \left(\frac{B}{H} + \frac{A}{R^2} H^\lambda \right) \\ & + \frac{A}{R^2} \left[\frac{U_{\lambda\lambda} + H_\lambda U_\lambda}{\sin^2 \Theta} + U_{\theta\theta} + (\cot \theta - H_\theta + \bar{H}_\theta) U_\theta \right] \quad (29a) \\ & + \frac{A}{R^2 \sin \Theta} [H_\lambda \bar{H}_\theta V - (2 \cot \theta + \bar{H}_\theta) V_\lambda] + 2\Omega V \cos \theta, \end{aligned}$$

$$\begin{aligned}
 V_i = & \frac{GH}{R} (\beta\kappa - \alpha\eta)_\theta - V \left(\frac{B}{H} + \frac{A}{R^2} H^\theta \right) \\
 & + \frac{A}{R^2} \left[\frac{V_{\lambda\lambda}}{\sin^2 \theta} + V_{\theta\theta} + (\cot \theta - H_\theta + 2\tilde{H}_\theta) V_\theta \right] \quad (29b) \\
 & + \frac{A}{R^2 \sin \theta} [2 \cot \theta U_\lambda - H_\lambda U_\theta - (\cot \theta - H_\theta) H_\lambda U] - 2\Omega U \cos \theta,
 \end{aligned}$$

and

$$R \sin \theta \zeta_i + U_\lambda - (V \sin \theta)_\theta = 0, \quad (30)$$

where $\alpha = 0.69$, $\beta = 0.9$, and

$$H^\lambda = \frac{H_{\lambda\lambda} + 1 + H^2}{\sin^2 \theta} + H_{\theta\theta} - H_\theta (H_\theta - \tilde{H}_\theta) + (H_\theta + \tilde{H}_\theta) \cot \theta, \quad (31a)$$

$$H^\theta = \frac{\tilde{H}_{\lambda\lambda} + 1}{\sin^2 \theta} + H_{\theta\theta} + H_\theta (\cot \theta - H_\theta + 2\tilde{H}_\theta), \quad (31b)$$

$$\left. \begin{aligned}
 \bar{H}_\theta &= H_\theta / H, \quad \bar{H}_{\theta\theta} = H_{\theta\theta} / H, \quad (\theta \rightarrow \lambda) \\
 \tilde{H}_\theta &= H_\theta + \mu \cos \theta / (1 + \mu \sin \theta),
 \end{aligned} \right\} \quad (32)$$

and

$$A = \frac{a}{2} LH(\lambda, \theta) (1 + \mu \sin \theta), \quad B = b \mu \sin \theta. \quad (33)$$

It may be mentioned that for $\alpha = \beta = 1$ and $A = B = 0$ the ocean tide equations (Equations 29 and 30) reduce to the considerably simpler classical Laplace tidal equations. Evidently, the complete COTEs require second derivatives ($H_{\lambda\lambda}$, $H_{\theta\theta}$) of the bottom topography, which can be assumed to exist without placing major restrictions on the realistic features of the bathymetry. It is interesting to note that those second derivatives in H^λ and H^θ act as modifying bottom-friction terms. A ridgelike ocean floor (say, $H_{\lambda\lambda} > 0$)

always adds to the bottom-friction terms $(U, V) \cdot B/H$, while a valley ($H_{\lambda\lambda} < 0$) always diminishes bottom friction.

Second-Order Arctic Tides

The COTES (Equations 29 and 30) become singular at the North Pole. For the intended numerical procedure, it is therefore advantageous to seek an approximate analytic solution around this singularity that can be matched together with the numerical solution at some appropriate colatitude. In fact, a unique "second-order arctic tide" solution can be determined for all three species of tide-generating potentials listed as Equations 12, 13, and 14, provided the ocean depth around the North Pole is assumed constant.

For constant depth, $H = H_0$, constant eddy viscosity, $A = A_0$, and constant bottom-friction coefficient, $B = B_0$, the COTES (Equations 29 and 30) assume the simpler form:

$$U_t = \frac{GH_0}{R \sin \theta} (\alpha\eta - \beta\xi)_\lambda + 2\Omega V \cos \theta - \frac{B_0}{H_0} U + \frac{A_0}{R^2 \sin^2 \theta} [U_{\lambda\lambda} - U + \sin \theta (\sin \theta U_\theta)_\theta - 2 \cos \theta V_\lambda], \quad (34a)$$

$$V_t = \frac{GH_0}{R} (\beta\xi - \alpha\eta)_\theta - 2\Omega U \cos \theta - \frac{B_0}{H_0} V + \frac{A_0}{R^2 \sin^2 \theta} [V_{\lambda\lambda} - V + \sin \theta (\sin \theta V_\theta)_\theta + 2 \cos \theta U_\lambda], \quad (34b)$$

and

$$\xi_t + \frac{1}{R \sin \theta} [U_\lambda - (V \sin \theta)] = 0. \quad (35)$$

The forcing equilibrium tides, η (Equations 12, 13, and 14), may be written in the unified complex form

$$\eta = \bar{\eta}(\lambda, \theta) e^{i\omega t}, \quad (36)$$

where

$$\eta = \eta_\nu(\lambda, \theta) = \begin{cases} K \sin^2 \theta e^{2\nu\lambda}, & (\nu = 2) & (37a) \\ K \sin 2\theta e^{\nu\lambda}, & (\nu = 1) & (37b) \\ K(3 \sin^2 \theta - 2) & & (37c) \end{cases}$$

With the substitution

$$(\eta, \zeta, U, V) = (\bar{\eta}, \bar{\zeta}, U, iV) e^{i\nu t} \quad (38)$$

one arrives at the following three complex differential equations in (λ, θ) :

$$\begin{aligned} \sigma U = & \frac{iGH_0}{R \sin \theta} (\beta \bar{\zeta} - \alpha \bar{\eta})_\lambda + 2\Omega V \cos \theta + i \frac{B_0}{H_0} U \\ & - \frac{iA_0}{R^2 \sin^2 \theta} [U_{\lambda\lambda} - U + \sin \theta (\sin \theta U_\theta)_\theta - 2i \cos \theta V_\lambda], \end{aligned} \quad (39a)$$

$$\begin{aligned} \sigma V = & \frac{GH_0}{R} (\alpha \bar{\eta} - \beta \bar{\zeta})_\theta + 2\Omega U \cos \theta + i \frac{B}{H_0} V \\ & - \frac{iA_0}{R^2 \sin^2 \theta} [V_{\lambda\lambda} - V + \sin \theta (\sin \theta V_\theta)_\theta - 2i \cos \theta U_\lambda], \end{aligned} \quad (39b)$$

and

$$\sigma \bar{\zeta} = \frac{1}{R \sin \theta} [iU_\lambda + (V \sin \theta)_\theta]. \quad (40)$$

The reduced Equations 39 and 40 may be solved for regular solutions by power series in $\sin \theta$ (essentially polar distance) of the form:

For $\nu = 2$ and $\nu = 0$,

$$\begin{aligned} \zeta &= \zeta_0(\lambda) + \zeta_1(\lambda) \sin \theta + \zeta_2(\lambda) \sin^2 \theta + \dots, \\ U &= U_0(\lambda) + U_1(\lambda) \sin \theta + U_2(\lambda) \sin^2 \theta + \dots, \end{aligned}$$

and

$$V = \cos \theta [V_0(\lambda) + V_1(\lambda) \sin \theta + V_2(\lambda) \sin^2 \theta + \dots];$$

} (41)

and for $\nu = 1$,

$$\begin{aligned} \zeta &= \cos \theta [\zeta_0(\lambda) + \zeta_1(\lambda) \sin \theta + \zeta_2(\lambda) \sin^2 \theta + \dots], \\ U &= \cos \theta [U_0(\lambda) + U_1(\lambda) \sin \theta + U_2(\lambda) \sin^2 \theta + \dots] \end{aligned}$$

and

$$V = V_0(\lambda) + V_1(\lambda) \sin \theta + V_2(\lambda) \sin^2 \theta + \dots$$

} (42)

By truncating the series expansions (Equations 41 and 42) after the second order in $\sin \theta$ and substituting these truncations into the Equations 39 and 40 up to the same quadratic power, one arrives after some lengthy but simple algebra at the following unique "second-order arctic tidal approximations." For semidiurnal tides ($\nu = 2$),

$$\begin{aligned} \eta &= K \sin^2 \theta e^{i(2\lambda + \sigma t)}, \\ \zeta &= 6K \sin^2 \theta e^{i(2\lambda + \sigma t)}, \\ U &= -2K \sigma R \sin \theta e^{i(2\lambda + \sigma t)}, \end{aligned}$$

and

$$V = -iK \sigma R \sin^2 \theta e^{i(2\lambda + \sigma t)},$$

} (43)

where

$$K = \alpha G H_0 K / [6\beta G H_0 + \sigma R^2 (2\Omega - \sigma) + i\sigma (6A_0 + B_0 R^2 / H_0)]; \quad (43a)$$

and for diurnal tides ($\nu = 1$),

$$\left. \begin{aligned} \eta &= K \sin 2\theta e^{i(\lambda + \sigma t)}, \\ \zeta &= 3\bar{K}_1 \sin 2\theta e^{i(\lambda + \sigma t)}, \\ U &= (\bar{K}_2 + 6\bar{K}_3 \sin^2 \theta) \cos \theta e^{i(\lambda + \sigma t)}, \end{aligned} \right\} (44)$$

and

$$V = i [\bar{K}_2 + 2(\bar{K}_3 + \bar{K}_1 \sigma R) \sin^2 \theta] e^{i(\lambda + \sigma t)},$$

where

$$\left. \begin{aligned} \bar{K}_3 &= \frac{K_{31}K_{33}(K_{22} - K_{12})}{K_{22}(K_{13}K_{31} - K_{11}K_{32}) - K_{12}(K_{31}K_{23} - K_{21}K_{32})}, \\ \bar{K}_2 &= \frac{1}{K_{12}} [K_{33} - \bar{K}_3(K_{13} - K_{11}K_{32}/K_{31})], \\ \bar{K}_1 &= -\bar{K}_3K_{32}/K_{31}; \end{aligned} \right\} (44a)$$

and

$$\left. \begin{aligned} K_{11} &= (6\beta GH_0 - \sigma^2 R^2) + i\sigma(6A_0 + B_0 R^2/H_0), \\ K_{12} &= -\Omega R, \\ K_{13} &= R(6\Omega - \sigma) + \frac{i}{R}(12A_0 + B_0 R^2/H_0), \\ K_{21} &= 6\beta GH_0 + 4i\sigma A_0, \\ K_{22} &= R(\sigma - 2\Omega) - \frac{i}{R}(2A_0 + B_0 R^2/H_0), \\ K_{23} &= 16iA_0/R, \\ K_{31} &= 2\sigma\Omega R^2, \\ K_{32} &= R(2\Omega - 3\sigma) + 3\frac{i}{R}(12A_0 + B_0 R^2/H_0), \\ K_{33} &= 2\alpha GH_0 K. \end{aligned} \right\} (44b)$$

For long period tides ($\nu = 0$),

$$\left. \begin{aligned} \eta &= -K(2 - 3 \sin^2 \theta) e^{i\sigma t}, \\ \zeta &= -2\bar{K}_1(2 - 3 \sin^2 \theta) e^{i\sigma t}, \\ U &= \bar{K}_2 \sin \theta e^{i\sigma t}, \end{aligned} \right\} (45)$$

and

$$V = -i\bar{K}_1 \sigma R \sin 2\theta e^{i\sigma t},$$

where

$$\begin{aligned}\tilde{K}_1 &= 4\sigma\Omega R^2 / [\sigma R^2 - i(2A_0 + B_0 R^2/H_0)], \\ \tilde{K}_2 &= -\tilde{K}_1 \tilde{K}_3,\end{aligned}$$

and

(45a)

$$\begin{aligned}\tilde{K}_1 &= -3\alpha GH_0 K [(6\beta GH_0 - \sigma^2 R^2 + \Omega R \tilde{K}_3) \\ &\quad + i\sigma(6A_0 + B_0 R^2/H_0)].\end{aligned}$$

It is important to note that the surprising uniqueness is achieved by requiring a regular integral at the North Pole (Equations 41 or 42) and by truncating the series of the solution and the differential equations after the second power of $\sin \theta$. Of course, without the second-order truncation, uniqueness can no longer exist. Undetermined coefficients become available to satisfy prescribed boundary data, say, at distant continental shorelines.

In the present global tide model, the arctic tides (Equations 43, 44, and 45) will be considered valid up to 1° colatitude (the first land occurs at colatitude 7° ; see Bathymetric Tables in Schwiderski, 1978a). For colatitudes 2° and 3° , a linear interpolation will be used to match the polar solution with the numerical solution computed south of 3° colatitude.

It is interesting to observe that if the Coriolis force and eddy dissipation are neglected ($\Omega = 0$, $A_0 = 0$), then the second-order arctic tides (Equations 43, 44, and 45) become exact global tides with the constants

$$\begin{aligned}K &= \alpha GH_0 K / [(6\beta GH_0 - \sigma^2 R^2) + i\sigma B_0 R^2/H_0], \\ \tilde{K}_1 &= 2K, \tilde{K}_2 = -2\sigma RK, \tilde{K}_3 = 0, \\ \tilde{K}_1 &= -3K, \tilde{K}_2 = 0, \tilde{K}_3 = 0.\end{aligned}$$

From Equations 43, 44, and 45, one concludes that all second-order arctic tides, ζ , vanish at the North Pole with the same order as their corresponding driving equilibrium tides η . Hence, only long-period tides exist at the North Pole.

Derivation of Discrete Ocean Tide Equations

The 1° by 1° Graded Grid System and Bathymetry

With the exception of Antarctica (south of colatitude $\theta = 168^\circ$), the entire (ocean and land) area of the globe is covered by a 1° by 1° grid system that is "graded" toward the poles. Each spherically rectangular mesh cell $S_{m,n}$ is bounded on the east and west by longitudes $\lambda_m = m^\circ$ and $\lambda_{m-\mu} = (m - \mu)^\circ$, respectively, and to the south and north by colatitudes $\theta_n = n^\circ$ and $\theta_{n-1} = (n - 1)^\circ$, respectively, so that

$$S_{m,n} = \left\{ (m - \mu)^\circ \quad \begin{matrix} (n - 1)^\circ \\ n^\circ \end{matrix} \quad m^\circ \right\}, \quad (46)$$

where

$$\left. \begin{array}{l} m = \mu, 2\mu, \dots, (360 \rightarrow 0) \\ \text{and} \\ n = 1, 2, \dots, 168. \end{array} \right\} \quad (47)$$

The "grading" parameter $\mu = \mu_n$ is defined by:

$$\left. \begin{array}{l} \mu = 1 \text{ for } n = 30 \text{ to } 150 \\ \mu = 2 \text{ for } n = 15 \text{ to } 29 \text{ and } n = 151 \text{ to } 168 \\ \mu = 4 \text{ for } n = 8 \text{ to } 14 \\ \mu = 8 \text{ for } n = 1 \text{ to } 7 \end{array} \right\} \quad (48)$$

The grading of the network toward the poles is necessary in order to maintain a more uniform mesh area for higher accuracy and stability (section, "Stability Analysis") of the discrete tide model. In fact, the grading equations (Equations 48) have been chosen in such a way that

$$\mu \sin n^\circ \geq 1/2 \text{ for } n = 4, 8, 15, 30, 150, 165; \quad (49)$$

i.e., the southern mesh size remains larger than half the equator mesh size. This important condition is violated for $n = 1^\circ, 2^\circ, 3^\circ$

and $n = 166^\circ, 167^\circ, 168^\circ$. However, in the preceding section it was pointed out that the numerically discrete tide model begins at colatitude $\theta = 4^\circ$. For colatitudes $\theta = 3^\circ$ and 2° , the numerical solution will be matched by linear interpolation to the second-order arctic-tide approximations derived in the preceding section, which are assumed to be useful up to colatitude $\theta = 1^\circ$. As will be shown in the section, "Stability Analysis," the slight violation of the condition in Equation 49 at the three southern colatitudes is not so severe as to affect the stability characteristics of the model. In any case, no need was apparent to justify an additional grading step, which is accompanied by an unnecessary, extra computational effort (next section).

In the global network defined above, land and ocean mesh cells are distinguished, respectively, by zero or nonzero depth data $H_{m,n}$ which will be assigned to each cell below. The "mathematical" boundaries of the oceans follow in an obviously zigzagging fashion the mesh lines of boundary cells.

The ocean-depth data collected by Smith *et al.* (1966) were rearranged and linearly interpolated to fit the new 1° by 1° graded grid system described above. The original data bank had to be corrected for obvious errors in continental and oceanic labeling, ocean and land signs, shorelines, and some exponents. All land elevations were set to zero, including all depth data less than 50 m. Furthermore, the following meshwise-disconnected border seas were excluded from consideration by assigning zero-depth values to their corresponding mesh cells: the Baltic, Kattegat, Irish, Mediterranean, Red, Japan, Sulu, and Ceram seas; the Hudson and Korean bays; and the Chihlian, Persian, and Californian gulfs.

All depth data $H_{m,n}$ are considered representative for the center of the cell $S_{m,n}$; i.e., for $m = \mu, 2\mu, \dots, 360$ and $n = 1, 2, \dots, 168$,

$$H_{m,n} = H(\lambda_m, \theta_n),$$

where $\lambda_m = (m - \mu/2)^\circ$ and $\theta_n = (n - 1/2)^\circ$.

The assigned minimum and maximum depth values were, respectively,

$$H_m = \min H(\lambda, \theta) = 50 \text{ m}, \quad (51)$$

$$H_M = \max H(\lambda, \theta) = 7,000 \text{ m}. \quad (52)$$

The averaged North Pole depth was found to be

$$H_0 = 3,600 \text{ m}, \quad (53)$$

which is needed to compute second-order arctic tides (section, "Second-Order Arctic Tides") for colatitude line $n = 1$.

The Discrete Ocean Tide Equations (DOTEs)

Following essentially the hydrodynamical numerical method of Hansen (1966) and Zahel (1970), the COTEs (Equations 29 and 30) may now be converted to an explicit finite-difference analog called "discrete ocean tide equations" (DOTEs). In agreement with the graded grid system defined in the preceding section, it is convenient to introduce the following notations:

$$\Delta\theta = \pi/360 = 1/2^\circ \text{ mesh size}, \quad (54)$$

$$\Delta\lambda = \mu\Delta\theta,$$

$$L = 2R\Delta\theta,$$

$$\Delta t = \text{time step to be specified}. \quad (55)$$

In a first step, all spacial derivatives of Equations 29 and 30 are replaced by divided central finite differences, using a Richardson (1922) staggered scheme. Accordingly, for a fixed oceanic mesh cell $S_{m,n}$ (Equation 46; $j = 1, 2, 3 \dots$)

$$U_{m,n}^{j+1} = U(\lambda_m(u), \theta_n(u), j\Delta t),$$

$$V_{m,n}^{j+1} = V(\lambda_m(v), \theta_n(v), j\Delta t),$$

and

$$\zeta_{m,n}^{j+1} = \zeta(\lambda_m(\zeta), \theta_n(\zeta), j\Delta t)$$

are computed, respectively, at the u -point of $S_{m,n}$

(56)

$$\lambda_m(u) = 2(m - \mu)\Delta\lambda, \theta_n(u) = (2n - 1)\Delta\theta, \quad (57a)$$

v-point of $S_{m,n}$

$$\lambda_m(v) = (2m - \mu)\Delta\lambda, \theta_n(v) = 2n\Delta\theta, \quad (57b)$$

and ζ -point of $S_{m,n}$

$$\lambda_m(\zeta) = \lambda_m(v), \theta_n(\zeta) = \theta_n(u), \quad (57c)$$

Undefined data are specified by arithmetic means of defined values. For example, needed U-data at v-points are defined by averages of U-values at adjacent u-points.

In the second part of the differencing process the resulting equations are integrated in time over a single time step, Δt , by using the following average integration rule ($U \rightarrow V \rightarrow \zeta$)

$$\int_{t_j}^{t_{j+1}} U(t) dt = \Delta t [\kappa U^{j+1} + (1-\kappa)U^j], \quad (58)$$

where

$$U^j = U(t_j), t_j = (j-1)\Delta t, j = 1, 2, \dots,$$

and κ = some differencing parameters, which usually satisfy the restriction

$$0 \leq \kappa \leq 1. \quad (59)$$

As will be seen, the resulting discrete ocean tide equations (DOTEs) are very sensitive to the choice of the differencing parameters, κ , and the time step, Δt . In fact, depending on the chosen values of κ and Δt , the DOTEs may be stable or unstable (section, "Stability Analysis") for any specified values of eddy viscosity, A, and bottom-friction coefficient, B. Moreover, different values of κ for Equations 29 and 30 and for the various point values of U, V, and ζ can be chosen so that the resulting DOTEs may become explicit or implicit. Considering the complexity of the ocean basin and the

large number of oceanic mesh cells, an explicit form for the DOTEs is here preferred.

After carrying out the described integration with the three (obvious) differencing parameters $\kappa = 0$, κ and, $\bar{\kappa}$, one arrives at the following explicit DOTEs. (For a more detailed derivation see Schwiderski, 1978b.)

$$\begin{aligned}
 [1 + \kappa A_{m,n}^4] U_{m,n}^{j+1} &= A_{m,n}^1 \sin \frac{\sigma \Delta t}{2} (2j - 1) \\
 &+ A_{m,n}^2 \cos \frac{\sigma \Delta t}{2} (2j - 1) + A_{m,n}^3 [\zeta_{m-\mu,n}^j - \zeta_{m,n}^j] \\
 &+ [1 - (1 - \kappa) A_{m,n}^4] U_{m,n}^j + A_{m,n}^5 U_{m+\mu,n}^j \\
 &+ A_{m,n}^6 U_{m-\mu,n}^j + A_{m,n}^7 U_{m,n+1}^j + A_{m,n}^8 U_{m,n-1}^j \\
 &+ A_{m,n}^9 [(V_{m,n}^j + V_{m,n-1}^j) - (V_{m-\mu,n}^j + V_{m-\mu,n-1}^j)] \\
 &+ A_{m,n}^{10} [(V_{m,n}^j + V_{m,n-1}^j) + (V_{m-\mu,n}^j + V_{m-\mu,n-1}^j)]. \quad (60a)
 \end{aligned}$$

$$\begin{aligned}
 [1 + \kappa B_{m,n}^4] V_{m,n}^{j+1} &= B_{m,n}^1 \cos \frac{\sigma \Delta t}{2} (2j - 1) \\
 &+ B_{m,n}^2 \sin \frac{\sigma \Delta t}{2} (2j - 1) \\
 &+ B_{m,n}^3 [\zeta_{m,n+1}^j - \zeta_{m,n}^j] + [1 - (1 - \kappa) B_{m,n}^4] V_{m,n}^j \\
 &+ B_{m,n}^5 [V_{m+\mu,n}^j + V_{m-\mu,n}^j] + B_{m,n}^6 V_{m,n+1}^j \\
 &+ B_{m,n}^7 V_{m,n-1}^j \\
 &+ B_{m,n}^8 [U_{m+\mu,n+1}^j - U_{m,n}^j] + B_{m,n}^9 [U_{m+\mu,n}^j - U_{m,n+1}^j] \\
 &+ B_{m,n}^{10} [U_{m+\mu,n+1}^j + U_{m,n}^j + U_{m+\mu,n}^j + U_{m,n+1}^j], \quad (60b)
 \end{aligned}$$

and

$$\begin{aligned}
 \zeta_{m,n}^{j+1} &= \zeta_{m,n}^j + \bar{\kappa} [C_n^1 (U_{m,n}^{j+1} - U_{m+\mu,n}^{j+1}) + C_n^2 V_{m,n}^{j+1} - C_n^3 V_{m,n-1}^{j+1}] \\
 &+ (1 - \bar{\kappa}) [C_n^1 (U_{m,n}^j - U_{m+\mu,n}^j) \\
 &+ C_n^2 V_{m,n}^j - C_n^3 V_{m,n-1}^j]. \quad (61)
 \end{aligned}$$

The coefficients of the DOTEs (Equations 60 and 61) are

$$\begin{aligned}
 A_{m,n}^1 &= A_{m,n} \cos 2\nu(m - \mu) \Delta\theta, \\
 A_{m,n}^2 &= A_{m,n} \sin 2\nu(n - \mu) \Delta\theta, \\
 A_{m,n}^3 &= \beta \Delta t G H(u) \Gamma_n(u) / L, \\
 A_{m,n}^4 &= 2a \frac{\Delta t}{L} \psi_n(u) \left[\omega_n(u) H(u) - \bar{H}(u) \right] \\
 &\quad + b \Delta t / \Gamma_n(u) H(u), \\
 A_{m,n}^5 &= a \frac{\Delta t}{L} \psi_n(u) \Gamma_n^2(u) H(u) \left[1 + \bar{H}(u) \right], \\
 A_{m,n}^6 &= a \frac{\Delta t}{L} \psi_n(u) \Gamma_n^2(u) H(u) \left[1 - H(u) \right], \\
 A_{m,n}^7 &= a \frac{\Delta t}{L} H(u) \left[\psi_n(u) + \frac{\mu \Delta \theta}{2} (2 + \Gamma_n(u)) \right. \\
 &\quad \left. \cdot \cos(2n - 1) \Delta\theta \right], \\
 A_{m,n}^8 &= a \frac{\Delta t}{L} H(u) \left[\psi_n(u) - \frac{\mu \Delta \theta}{2} (2 + \Gamma_n(u)) \right. \\
 &\quad \left. \cdot \cos(2n - 1) \Delta\theta \right], \\
 A_{m,n}^9 &= a \frac{\Delta t}{L} \Gamma_n(u) H(u) \left[\psi_n(u) \hat{H}(u) - \frac{\mu \Delta \theta}{2} (3 + 2\Gamma_n(u)) \right. \\
 &\quad \left. \cdot \cos(2n - 1) \Delta\theta \right],
 \end{aligned}
 \tag{62a}$$

and

$$A_{m,n}^{10} = -a \frac{\Delta t}{L} \Gamma_n(u) H(u) \bar{H}(u) \left[\psi_n(u) \hat{H}(u) - \frac{\mu \Delta \theta}{2} \right. \\ \left. \cos(2n-1) \Delta \theta \right] + \frac{\Delta t}{2} \Omega \cos(2n-1) \Delta \theta, \quad (62a)$$

where

$$A_{m,n} = -4 \frac{\alpha G}{\sigma R} K H(u) \sin \frac{\sigma \Delta t}{2} \begin{cases} \sin(2n-1) \Delta \theta, & \nu = 2 \\ \cos(2n-1) \Delta \theta, & \nu = 1 \\ 0, & \nu = 0 \end{cases}$$

and

$$\Gamma_n(u) = 1/\mu \sin \theta_n(u); \quad \psi_n(u) = \frac{1}{2} (1 + 1/\Gamma_n(u)), \quad (63a)$$

$$\omega_n(u) = 1 + \Gamma_n^2(u);$$

$$B_{m,n}^1 = B_{m,n} \cos \nu(2m - \mu) \Delta \theta,$$

$$B_{m,n}^2 = -B_{m,n} \sin \nu(2m - \mu) \Delta \theta,$$

$$B_{m,n}^3 = \beta \Delta t G H(v) / L,$$

$$B_{m,n}^4 = 2a \frac{\Delta t}{L} \psi_n(v) \left[\omega_n(v) H(v) - \tilde{H}(v) \right] \\ + b \Delta t / \Gamma_n(v) H(v), \quad (62b)$$

$$B_{m,n}^5 = a \frac{\Delta t}{L} \psi_n(v) \Gamma_n^2(v) H(v),$$

$$B_{m,n}^6 = a \frac{\Delta t}{L} H(v) \left[\psi_n(v) (1 - \hat{H}(v)) \right]$$

$$+ \frac{\mu \Delta \theta}{4} (3 + 2\Gamma_n(\nu)) \cos 2n\Delta\theta],$$

$$B_{m,n}^7 = a \frac{\Delta t}{L} H(\nu) \left[\psi_n(\nu) (1 + \hat{H}(\nu)) - \frac{\mu \Delta \theta}{4} (3 + 2\Gamma_n(\nu)) \cos 2n\Delta\theta \right],$$

$$B_{m,n}^8 = a \frac{\Delta t}{L} \Gamma_n(\nu) \psi_n(\nu) H(\nu) [2\mu \Delta \theta \Gamma_n(\nu) \cos 2n\Delta\theta - \bar{H}(\nu)],$$

$$B_{m,n}^9 = a \frac{\Delta t}{L} \Gamma_n(\nu) \psi_n(\nu) H(\nu) [2\mu \Delta \theta \Gamma_n(\nu) \cos 2n\Delta\theta + H(\nu)],$$

and

$$B_{m,n}^{10} = -a \frac{\Delta t}{L} \Gamma_n(\nu) \psi_n(\nu) H(\nu) \bar{H}(\nu) [\mu \Delta \theta \Gamma_n(\nu) \cos 2n\Delta\theta + \hat{H}(\nu)] - \frac{\Delta t}{2} \Omega \cos 2n\Delta\theta,$$

where

$$B_{m,n} = -4 \frac{\alpha G}{\sigma R} KH(\nu) \sin \frac{\sigma \Delta t}{2} \begin{cases} 2 \sin 4n\Delta\theta, & \nu = 2 \\ \cos 4n\Delta\theta, & \nu = 1 \\ 6 \sin 4n\Delta\theta, & \nu = 0 \end{cases}$$

and

(62b)

$$\Gamma_n(v) = 1/\mu \sin \theta_n(v); \quad \psi_n(v) = \frac{1}{2} (1 + 1/\Gamma_n(v)), \quad (63b)$$

$$\omega_n(v) = 1 + \Gamma_n^2(v);$$

$$C_n^{(1)} = \frac{\Delta t}{L} \Gamma_n(u),$$

$$C_n^{(2)} = \mu \frac{\Delta t}{L} \Gamma_n(u) \sin 2n\Delta\theta,$$

and

$$C_n^{(3)} = \mu \frac{\Delta t}{L} \Gamma_n(u) \sin 2(n-1)\Delta\theta.$$

(64)

In these coefficients, the following depth functions were used at u-points:

$$H_{m,n}(u) = \frac{1}{2} [H_{m,n} + H_{m-\mu,n}],$$

$$\bar{H}_{m,n}(u) = \frac{1}{4H_{m,n}(u)} [H_{m-\mu,n}(u) - H_{m-\mu,n}(u)],$$

$$\hat{H}_{m,n}(u) = \frac{1}{4H_{m,n}(u)} [H_{m,n-1}(u) - H_{m,n+1}(u)],$$

$$\begin{aligned} \bar{H}_{m,n}(u) = H_{m,n}(u) \left\{ \omega_n(u) - 2\Gamma_n^2(u) [\bar{H}_{m,n}^2(u) + (\mu\Delta\theta)^2] \right. \\ \left. + \mu\Delta\theta\psi_n(u) \cos(2n-1)\Delta\theta [(3 + 2\Gamma_n(u))\hat{H}_{m,n}(u) \right. \\ \left. - \mu\Delta\theta\Gamma_n(u) \cos(2n-1)\Delta\theta] \right\} \\ - \frac{1}{2} [\Gamma_n^2(u) (H_{m+\mu,n}(u) + H_{m-\mu,n}(u)) \\ + (H_{m,n+1}(u) + H_{m,n-1}(u))]; \end{aligned} \quad (65a)$$

and at v-points

$$\begin{aligned}
 H_{m,n}(v) &= \frac{1}{2} [H_{m,n} + H_{m,n+1}], \\
 \bar{H}_{m,n}(v) &= \frac{1}{4H(v)} [H(v)_{m+\mu,n} - H(v)_{m-\mu,n}], \\
 \dot{H}_{m,n}(v) &= \frac{1}{4H(v)} [H(v)_{m,n-1} - H(v)_{m,n+1}], \\
 \ddot{H}_{m,n}(v) &= H(v)_{m,n} \left\{ \omega_n(v) - 2[\dot{H}^2(v)_{m,n} + (\mu\Delta\theta)^2\Gamma_n^2(v)] \right. \\
 &\quad \left. + \mu\Delta\theta\psi_n(v)\dot{H}_{m,n}(v) [3 + \Gamma_n(v)] \cos 2n\Delta\theta \right\} \\
 &\quad - \frac{1}{2}\Gamma_n^2(v) (H(v)_{m+\mu,n} + H(v)_{m-\mu,n}) \\
 &\quad + (H(v)_{m,n+1} + H(v)_{m,n-1}).
 \end{aligned} \tag{65b}$$

Obviously, due to the introduction of the novel depth-dependent eddy viscosity (Equation 6) the COTEs and the DOTEs (Equations 29, 30 and 60, 61) are considerably more involved than the corresponding equations used by Zabel (1970, 1973, 1975) and Estes (1975). This results in drastically increased computer time, memory, and cost.

For $\kappa = 0$ and $\bar{\kappa} = 1$, the finite-difference scheme coincides with the technique used, e.g., by Hansen (1966), Zabel (1970, 1973, 1975), and Estes (1975, 1977). Extensive exploratory computations were carried out by the author with numerous κ and $\bar{\kappa}$ values within the ranges $0 \leq \bar{\kappa} \leq 1.5$ and $0.5 \leq \kappa \leq 1$. The computations produced no drastic differences, provided the eddy and bottom-friction coefficients a and b and the time step Δt were suitably chosen within their respective stability constraints (section, "Stability Analysis"). Finally, it was decided to use the values

$$\kappa = \bar{\kappa} = 1 \quad (66)$$

because they yielded a preferable stability and seemingly best results. Moreover, this deviation from the Hansen-Zahel method became most significant for the hydrodynamical interpolation of empirical tidal data described in Part II (Schwiderski, 1979b). Indeed, this novel technique uses the special property that for $\bar{\kappa} = 1$ the bottom-friction coefficient, b , which enters only in A^4 and B^4 (Equations 62) becomes essentially a scaling multiplier of $U_{m,n}^{j+1}$ and $V_{m,n}^{j+1}$ in Equations 60a and 60b. Thus, together with $\bar{\kappa} = 1$ in Equation 61, the bottom-friction coefficient can easily be adjusted locally to match more closely prescribed tidal data.

With κ and $\bar{\kappa}$ specified by Equation 66, the DOTEs (Equations 60 and 61) still contain the parameters a , b , and Δt , which remain at one's disposal within their respective stability ranges (section, "Stability Analysis"). They will be utilized to achieve best results by trial-and-error computations. The DOTEs (Equations 60 and 61) can be applied to all oceanic mesh cells $S_{m,n}$ with $m = \mu, 2\mu, \dots, 360$ and $n = 4, 5, \dots, 168$ sweeping across the globe from $n = 4$ to $n = 168$. This procedure can be executed, provided suitable initial and lateral boundary data (next section) are prescribed. At colatitude line $n = 4$, the numerical solution is matched to the second-order arctic solution (section, "Second-Order Arctic Tides") by the linear interpolation ($m = \mu, 2\mu, \dots, 360$).

$$\left. \begin{aligned} U_{m,8}^{j+1} &= \frac{1}{3} [2U_{m,4}^{j+1} + U_{m,1}^{j+1}] \\ U_{m,2}^{j+1} &= \frac{1}{3} [U_{m,4}^{j+1} + 2U_{m,1}^{j+1}] \end{aligned} \right\} (U \rightarrow V \rightarrow \zeta) \quad (67)$$

where $U_{m,1}^{j+1}$, $V_{m,1}^{j+1}$ and $\zeta_{m,1}^{j+1}$ are computed by Equations 43, 44, or 45. For colatitude lines $n = 7, 14, 29, 150$, spacially corresponding data (U, V, ζ) on $n = 8, 15, 30, 151$ (see Equation 49) are defined by linear interpolation. Vice versa, for $n = 8, 15, 30, 151$, spacially corresponding values (U, V, ζ) on $n = 7, 14, 29, 150$ are also defined by linear interpolation.

Lateral-Boundary, Initial, and Final Data

In order to complete the ocean-tide model, the DOTEs (Equations 60 and 61) must be supplemented by suitable lateral-boundary and initial values. In turbulent flow situations, the mathematical boundary conditions usually preferred are (a) no-flow across the ocean shorelines and (b) free-slip along the ocean shorelines. It is clearly at this point that the great attractiveness of Richardson's (1922) staggered, finite-difference scheme (preceding section) manifests itself in the practical simplicity with which the no-flow and free-slip (or no-slip) boundary conditions can be worked into the model. In fact, if $S_{m,n}$ is an oceanic boundary cell, then, by definition (section, "The $1^\circ \times 1^\circ$ Graded Grid System and Bathymetry"), the zig-zagging mathematical boundary lines follow only mesh lines and pass only through velocity (u and/or v) points. The no-flow condition (a) is implemented by declaring at those points

$$U_{m,n}^{j+1} = 0 \text{ and/or } V_{m,n}^{j+1} = 0, \quad (68)$$

respectively. If, say, the v -point of $S_{m,n}$ is oceanic and the v -points of $S_{m-\mu,n}$ and/or $S_{m+\mu,n}$ are terrestrial, then the free-slip condition (b) is satisfied by reflectively setting

$$V_{m-\mu,n}^{j+1} = +V_{m,n}^{j+1} \text{ and/or } V_{m+\mu,n}^{j+1} = +V_{m,n}^{j+1}, \quad (69)$$

respectively. (If the no-slip condition is imposed, then the (+) signs in Equation 69 must be changed to (-) signs.)

The mathematical boundary conditions (a) and (b) were applied by Hansen (1966), Zahel (1970, 1973, 1975), Estes (1975, 1977), and others. In the present model, both the free-slip and no-slip conditions were tested. The computer experiments indicated slightly better results for the free-slip condition, which was then adopted. Physically, this condition is more plausible in turbulent flows which have only very thin boundary layers (see, e.g., Schlichting, 1968). Furthermore, the free-slip condition is consistent with the bottom boundary assumption specified in the section, "The Continuous Ocean Tide Equations (COTEs)" (b,3).

The construction of the M_2 tide was started at $j = 1$ ($t_1 = 0$) with an ocean completely at rest; i.e., with the initial values ($m = \mu, 2\mu, \dots, 360; n = 1, 2, \dots, 168$)

$$U_{m,n}^1 = V_{m,n}^1 = \zeta_{m,n}^1 = 0. \quad (70)$$

The computations were carried over a prescribed number of time steps, $j = J$ (mostly a quarter period), and then printed for inspection of the results. With or without program and/or parameter changes, the computations were restarted, using the latest or any earlier taped output instead of the initial values (Equation 70). Occasionally, it was beneficial to speed up an unwanted slow decay of transient eigenmodes by "negatively" averaging the output data of half a period time difference; i.e., by setting

$$U^J = \frac{1}{2} (U^J + U^{J-2J}), \quad U \rightarrow V \rightarrow \zeta, \quad (71)$$

where $\sigma \Delta t J = \pi$. This simple procedure diminishes all undesirable eigenmodes of lower frequency than the forced frequency, σ , and, similarly, also most higher frequency modes. The negatively averaged data (Equation 71) represent obviously improved initial data.

Two output tidal elevations $2J$ -time steps apart (mostly a quarter-period apart),

$$\left. \begin{aligned} \zeta_{m,n}^J &= \xi_{m,n} \cos [\sigma \Delta t J - \delta_{m,n}] \\ \text{and} \\ \zeta_{m,n}^{J-2J} &= \xi_{m,n} \cos [\sigma \Delta t (J - 2J) - \delta_{m,n}], \end{aligned} \right\} \quad (72)$$

were used to compute the tidal "amplitudes"

$$\xi_{m,n} = [\xi_1^2 + \xi_2^2]^{\frac{1}{2}} \quad (73)$$

and "phases"

$$\delta_{m,n} = \arctan y/x \quad (= 0 \text{ for } x = y = 0), \quad (74)$$

where

$$\xi_1 = (\zeta_{m,n}^{J-2J} + \zeta_{m,n}^J) / 2 \cos \sigma \Delta t J, \quad (75)$$

$$\xi_2 = (\zeta_{m,n}^{J-2J} - \zeta_{m,n}^J) / 2 \sin \sigma \Delta t J,$$

$$y = \xi_1 \sin \sigma \Delta t (J - J) - \xi_2 \cos \sigma \Delta t (J - J),$$

and

$$x = \xi_1 \cos \sigma \Delta t (J - J) + \xi_2 \sin \sigma \Delta t (J - J).$$

In the finished product, i.e., when all (unforced) transient eigenmodes have satisfactorily decayed, the amplitudes (Equation 73) and phases (Equation 74) become essentially independent of time and undergo no further variation of significance after continued computations.

In the M_2 -tide model, the computed convergence toward the steady state of the amplitudes and phases was found to be generally oscillating. So the integration process could safely be terminated when the amplitudes and phases over most ocean areas varied by less than 2 cm and 3° , respectively. The convergence was slightly less complete in coastal cells where the tidal elevations are extremely large and vary rapidly from degree to degree.

In order to follow the convergence of the computer program more closely, the squared tidal-amplitude sum

$$\xi_n^2 = \sum_{m=\mu}^{360} \xi_{m,n}^2 \quad (77)$$

was computed and printed for each fixed colatitude line $n = 4, 5, \dots, 168$. To compute the amplitudes $\xi_{m,n}$ in Equation 77, Equations 73 and 75 were used for $2J = 1$ and $J = j + 1$; i.e., for two consecutive time steps in connection with Equation 61. In this measure (Equation 77), the convergence was carried to almost three significant figures for all n .

Stability Analysis

A rigorous stability analysis of the homogeneous DOTEs (Equations 60 and 61) is, of course, not possible. However, under the assumption of constant coefficients A , B , and C , the simplified DOTEs possess Fourier-type eigensolutions (Equation 88) that permit a local stability analysis of the difference system. As is well known (see, e.g., Richtmyer, 1957), such a local stability analysis produces stability limits that are usually sufficient for computational purposes. Indeed, computer experiments showed that the stability limits so derived below were scrupulously binding for the success of the integration. The following analysis is an expanded version of the investigation presented by Zahel (1970).

In detail, the following simplifications may be assumed:

- (a) $b = 0$; i.e., no bottom friction
- (b) $\Omega = 0$; i.e., no Coriolis force
- (c) For an arbitrary but fixed mesh cell (see Equations 62–65),

$$\Gamma = \Gamma_n(u) = \Gamma_n(v) = 1/\mu \sin \theta = \text{locally constant,}$$

$$\psi = \psi_n(u) = \psi_n(v) = 1/2 (1 + 1/\Gamma), \quad (78)$$

$$\omega = \omega_n(u) = \omega_n(v) = 1 + \Gamma^2;$$

and

$$H = H_{n,n}(u) = H_{n,n}(v) = \text{locally constant,} \quad (79)$$

$$\bar{H}_{n,n}(u) = \hat{H}_{n,n}(u) = \tilde{H}_{n,n}(u) = 0, (u \rightarrow v).$$

It may be mentioned that the assumptions (a) and (b) have been made in order to display more clearly the most important stability characteristics of the DOTEs that are due to eddy dissipation and to the differencing parameters, κ and $\bar{\kappa}$. It is relatively easy to show that the bottom friction is always stabilizing, while the Coriolis force (in the present differencing scheme) is slightly destabilizing.

For the following derivations, it is helpful to introduce some specified reference values θ_r , H_r , (consistent with Equations 78 and 79) Γ_r , ψ_r , ω_r , and

$$\alpha_r = \frac{1}{\psi_r} \left(\frac{G}{\omega_r H_r} \right)^{1/2}, \quad \Delta t_r = L / (\omega_r H_r G)^{1/2}. \quad (80)$$

Finally, the following relative quantities may be introduced:

$$\begin{aligned} \bar{\psi} &= \psi / \psi_r, \quad \bar{\omega} = \omega / \omega_r, \quad h = H / H_r, \\ \tau &= \Delta t / \Delta t_r, \quad \epsilon = \alpha / \alpha_r. \end{aligned} \quad (81)$$

For example, in this notation the eddy viscosity, A (Equation 6), assumes the form

$$A = \epsilon \alpha_r \psi H L, \quad (82)$$

where ϵ is the "dimensionless eddy coefficient."

The M_2 -tide is computed with the reference values

$$\theta_r = 30^\circ, \quad H_r = 7259.84 \text{ m}, \quad (83)$$

so that

$$\left. \begin{aligned} \psi_r &= 3/4, \quad \alpha_r = 0.021\,919\,2 \text{ sec}^{-1}, \\ \omega_r &= 5, \quad \Delta t_r = 186.309 \text{ sec}, \\ 180\sigma\Delta t_r/\pi &= 1.5^\circ, \quad J_p = 360^\circ/1.5^\circ = 240, \end{aligned} \right\} \quad (84)$$

where J_p is the number of time steps required to integrate through one tidal period with $\Delta t = \Delta t_r$. Due to the grading of the grid system (Equation 49), one has almost everywhere ($n \neq 1, 2, 3$, and $166, 167, 168$)

$$1 \leq \bar{\psi} \leq \frac{3}{4}, \quad 1 \geq \bar{\omega} \geq \frac{2}{5}. \quad (85)$$

Similarly, due to the cutoff depth data (Equations 50, 51), one has the limits

$$0.0065 < h < 1. \quad (86)$$

Several other reference values within the stability limits have been explored. Particularly extensive computations were carried out with $\Delta t_r = 248.412$ sec (so that $J_p = 180$), but the above reference values appeared to yield the best results.

With the simplifications and notations above, the coefficients (Equations 62–65) of the homogeneous DOTEs (Equations 60 and 61) become:

$$\left. \begin{aligned} A^1 &= A^2 = B^1 = B^2 = 0, \\ A^3 &= \Gamma B^3 = \beta GH \Gamma \Delta t / L, \\ A^4 &= B^4 = 2h\epsilon\tau\bar{\psi}\bar{\omega}, \\ A^5 &= A^6 = B^5 = B^6 = h\epsilon\tau\bar{\psi}/\omega_r, \\ A^7 &= A^8 = B^7 = \Gamma^2 A^5, \\ A^9 &= A^{10} = B^8 = B^9 = B^{10} = 0, \\ C^1 &= \Gamma \Delta t / L, C^2 = C^3 = \Delta t / L. \end{aligned} \right\} \quad (87)$$

The reduced DOTEs (with constant coefficients) yield the Fourier-type eigensolutions

$$\left. \begin{aligned} U_{m,n}^i &= U_0 d^i e^i [\gamma_1 (2m - 2\mu) \Delta\lambda + \gamma_2 (2n - 1) \Delta\theta], \\ V_{m,n}^i &= V_0 d^i e^i [\gamma_1 (2m - \mu) \Delta\lambda + \gamma_2 (2n - 1) \Delta\theta], \\ \text{and} \\ \zeta_{m,n}^i &= \zeta_0 d^i e^i [\gamma_1 (2m - \mu) \Delta\lambda + \gamma_2 (2n - 1) \Delta\theta]. \end{aligned} \right\} \quad (88)$$

with an arbitrary wave vector (γ_1, γ_2) and some nonzero amplitude vectors (U_0, V_0, ζ_0) , provided the eigenvalue d satisfies the cubic characteristic equation

$$\begin{vmatrix} (A_{11} - dA_{10}) & 0 & A_{13} \\ 0 & (A_{22} - dA_{10}) & A_{23} \\ (1 - \kappa + \kappa d)A_{31} & (1 - \kappa + \kappa d)A_{32} & (1 - d) \end{vmatrix} = 0, \quad (89)$$

where (after some algebra)

$$\left. \begin{aligned} A_{10} &= 1 + \kappa A^4 = 1 + 2\kappa h\epsilon r\bar{\psi}\bar{\omega}, \\ A_{11} &= A_{22} = A_{10} - 2A^4 s^2, \\ \text{and} \\ A_{12}A_{31} + A_{13}A_{23} &= -4\beta h\bar{\omega}r^2 s^2 \end{aligned} \right\} \quad (90)$$

with

$$0 \leq s^2 \leq \frac{\Gamma^2 \sin^2 \gamma_1 \Delta\theta + \sin^2 \gamma_2 \Delta\theta}{\Gamma^2 + 1} \leq 1. \quad (91)$$

The cubic characteristic Equation 89 yields the three eigenvalues ($d_0, d = d_1, d_2$)

$$d_0 = 1 - 4h\epsilon r\bar{\psi}\bar{\omega}s^2/A_{10} \quad (92)$$

and

$$dA_{10} = A_{10} - 2hr\bar{\omega}s^2 A_{01} \pm 2irs [h\bar{\omega}(\beta A_{10} - h\bar{\omega}s^2 A_{01}^2)]^{1/2}, \quad (93)$$

where

$$A_{01} = \epsilon\bar{\psi} + \beta\bar{\kappa}r. \quad (94)$$

The DOTEs will be stable, provided

$$|d_k| \leq 1 \text{ for } k = 0, 1, 2. \quad (95)$$

Under the strict inequality of Equation 95, the three eigenvalues $d_0, d_1,$ and d_2 define three decaying eigenwaves represented by Equations 88. Since d_0 is real, the corresponding eigenwave is a standing wave with no phase shift if $d_0 \geq 0$. The other two eigenvalues d_1 and d_2 define a pair of eigenwaves progressing in opposite directions with the same decay and dispersion rates, provided

$$\beta A_{10} \geq h\bar{\omega}s^2 A^2_{01}. \quad (96)$$

This condition holds true for all $0 \leq s \leq 1$ (Equation 91); i.e., for all wave vectors (γ_1, γ_2) if and only if

$$\beta A_{10} \geq h\bar{\omega}A^2_{01}. \quad (97)$$

If this condition fails, then there exist some short waves with large wave numbers, γ_1 and γ_2 , which become standing waves of different decay rates. However, all sufficiently long waves remain dispersively progressing and decaying at the same rates.

It seems physically plausible to treat all long and short waves equally and, hence, to impose the conditions of Equations 95 and 97 on the free parameters, ϵ , τ , κ , and $\bar{\kappa}$. Using Equations 93, 94, 95, and 97, one finds

$$|d_1|^2 = |d_2|^2 = 1 - 4h\tau\bar{\omega}s^2 [\epsilon\bar{\psi} - (1 - \bar{\kappa})\beta\tau] / A_{10} \quad (98)$$

with

$$|d_1|^2 = |d_2|^2 = d_0 \text{ for } \bar{\kappa} = 1. \quad (99)$$

For $\bar{\kappa} < 1$, the stability condition requires

$$\epsilon\bar{\psi} \geq (1 - \bar{\kappa})\beta\tau; \quad (100)$$

i.e., a minimum of eddy viscosity is necessary for stability. However, for $\bar{\kappa} = 1$, no minimum eddy viscosity is required, which explains the choice made here (Equation 66) and by Zahel (1970, 1973, 1975) and Estes (1975, 1977).

For the chosen value $\bar{\kappa} = 1$, the stability condition is satisfied for all, s , and all eigenvalues d_0 , d_1 , and d_2 , when

$$4h\tau\bar{\omega} \leq A_{10}; \quad (101)$$

i.e., when

$$\tau = \frac{\Delta t}{\Delta t_r} \leq \frac{1}{2} (2 - \kappa) \epsilon h \bar{\psi} \bar{\omega}, \quad (102)$$

provided (Equation 97 in explicit form) also

$$\frac{\beta}{h \bar{\omega}} \geq \beta^2 \tau^2 + 2\beta \epsilon \tau \bar{\psi} (1 - \kappa) + \epsilon^2 \bar{\psi}^2. \quad (103)$$

The obviously increased stability limits imposed by both conditions explain the choice of $\kappa = 1$ made here for the present tide model (Equation 66) in deviation from the value $\kappa = 0$ used by Zahel and Estes.

With $\beta = 0.90$ (Equation 17) and the possible values of $h = 1$ and, simultaneously, $\bar{\psi} = \bar{\omega} = .1$ (Equations 85, 86), one finds from Equations 102 and 103 for $\kappa = 1$ and $\tau = 1$ the allowable range for the dimensionless eddy coefficient, ϵ :

$$0 \leq \epsilon \leq 0.3 (\Delta t = \Delta t_r). \quad (104)$$

The same range holds also for the southern three colatitude lines $n = 166, 167, 168$, which violate the condition of Equation 49, but for which the relative depth, h , falls sufficiently below unity. The upper limit on ϵ could be raised somewhat by considering the simultaneous values of $\bar{\psi}$, $\bar{\omega}$, and h on each colatitude $n = 4, 5, \dots, 168$ separately. In order to obtain the best possible tidal field, extensive trial-and-error computations led to the choice

$$\Delta t = \Delta t_r = 186.309 \text{ sec and } \epsilon = 0.075. \quad (105)$$

This final choice completes the detailed parameter specifications of the M_2 tide model.

At this point, it may be noticed that the stability requirement for the DOTEs restricts the possible amount of eddy dissipation. As is physically plausible, the finite-differencing parameters, κ and τ , the mesh size, L , and depth, H , the time step, Δt , and the dimensionless eddy coefficient, ϵ , are intimately related to each other.

Trial-and-error computations are needed to select those parameters for best results. It is particularly important to observe that (especially for $\kappa = 1$) the rates of decay (Equations 92, 98, and 99) of all eigenwaves depend directly on the product $h\epsilon$. Accordingly, for fixed ϵ , waves in deep ($h \approx 1$) ocean basins decay faster than in shallow ($h \ll 1$) regions if bottom friction is negligible.

It is obviously this physically realistic phenomenon that led to the introduction of the novel depth-dependent eddy viscosity, A , defined by Equations 6 or 82. For a depth-independent eddy viscosity, one has $h\epsilon = \text{constant}$, in which case waves would decay at the same rate in deep or shallow (see next section) oceans, even though no bottom friction is present. Following Zahel (1970, 1973, 1975) and Estes (1975, 1977), the present tide model also used at first a constant eddy viscosity with rather disappointing results caused by the strongly varying bathymetry.

It is interesting to note that for the limiting case of Equation 97; i.e., for

$$\beta A_{10} = h\bar{\omega} A^2_{01}, \quad (106)$$

Equation 93 assumes the simple form

$$dA_{01} = A_{01} - 2\beta\tau s^2 \pm 2i\beta\tau s(1 - s^2)^{1/2}. \quad (107)$$

Hence, for the north-east waves under 45° with wave numbers (Equation 91),

$$\gamma_1 = \gamma_2 = \gamma, s^2 = \sin^2 \gamma \Delta \theta, \quad (108)$$

and ($\kappa = \bar{\kappa} = 1$)

$$d = \frac{\epsilon\bar{\psi} + \beta\tau e^{\pm 2i\gamma\Delta\theta}}{\epsilon\bar{\psi} + \beta\tau} = d_0 + d_1 e^{\pm 2i\gamma\Delta\theta}. \quad (109)$$

Hence, in this case, the eigenvalues d_1 and d_2 lie on the circle

$$|d - d_c| = d_r, d_c + d_r = 1 \quad (110)$$

as illustrated in Figure 2.

Discussion of the Tide Model

Discrete Versus Continuous Ocean-Tide Equations

In the following discussion it may be contended that discrete ocean tide equations (DOTEs, Equations 60 and 61) reflect the physical reality of ocean tidal currents more perfectly and perceptibly than the corresponding continuous equations (COTEs, Equations 29 and 30). Although the latter follow from the former by a "formal" limit process, it is neither technically feasible nor theoretically desirable to seek convergence of the discrete solution to the continu-

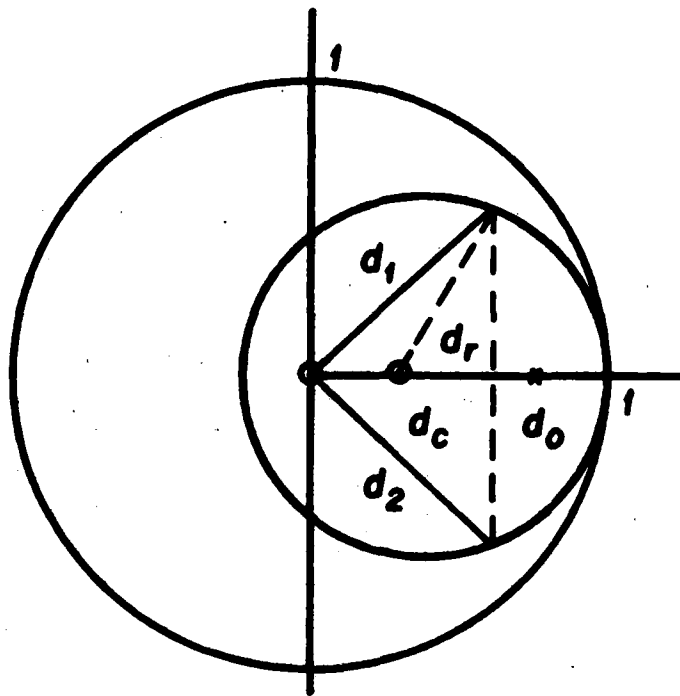


Figure 2. Illustration of eigenvalues d_0 , d_1 , and $d_2 = \bar{d}_1$, in circle $|d - d_c| \leq d_r$.

ous integral. In fact, in fluid-flow problems of global dimensions, it is not possible to approximate the conditions of the continuous case to any reasonable degree. Even with future computer technology, it will not be meaningful to refine significantly, for instance, the 1° by 1° grid system defined in the section, "The $1^\circ \times 1^\circ$ Graded Grid System and Bathymetry," which, with its 100-km mesh size, is far from being anywhere near a continuous description. Any attempt to refine the grid system would have to be matched by an improved bathymetry which requires worldwide *in situ* measurements.

From the theoretical point of view, it is equally superfluous to seek an ϵ -approximation of the continuous situation, which in fact is only vaguely defined (section, "The Navier-Stokes Equations of Averaged Turbulent Flow.") In laminar viscous flow theory, such notions as particle (point) velocity and pressure, as well as the Navier-Stokes equations, are all derived from physically sound discrete (finite-difference) definitions by a formal limit procedure; i.e., by simply assuming the existence of the limit values (see, e.g., Schlichting, 1968; Whitaker, 1968). While this assumption is well justified in most laminar flow problems, it is well known today (see, e.g., Ladyzhenskaya, 1969) that, in general, even laminar motions must be sought in the class of generalized (distribution) functions. Hence, velocities, pressure, and their derivatives do not exist in the ordinary sense (pointwise); only their "functionals" (effects such as mass fluxes, forces, momenta) are physically defined.

The ambiguity of continuous flow models becomes much more apparent in the critical laminar regime. Experiments (e.g., Busse and Whitehead, 1971) and theory (e.g., Schwiderski, 1972) have clearly established that, when given characteristic flow parameters (dimensions, velocities, etc.) exceed certain critical values, the corresponding, uniquely existent laminar motions become unstable and bifurcate into laminar flows in infinitely many different shapes. The classical laminar boundary and initial conditions are no longer sufficient to specify a unique motion. The situation seems to be governed by hysteresis and pure chance rather than by rigorous physical selection principles.

Critical laminar motions become still more microscopically undefinable when the corresponding characteristic flow parameters (as the global dimensions of ocean currents) exceed further supercritical points and the motions go turbulent. The statistical approach underlying the "time-averaging" process to derive the so-called Navier-Stokes equations of mean turbulent flow (Equations 1 and 2) is entirely formal and vague (see, e.g., Schlichting, 1968). For example, what velocity (particle, point, etc.) is averaged over what time interval? In this respect, the present periodic tidal motions are clearly the most illuminating of the problems at hand. If one averages (as usually meaningful) over a "sufficiently" long time span (say, longer than the tidal periods), then the averaged velocity should approach zero, which is obviously not of interest.

Evidently, turbulent particle velocities manifest themselves statistically through their integrated (macroscopic) physical effects, such as mass fluxes. Hence, the proper mathematical representation of turbulent motions should be sought in the class of generalized functions. Since the product of generalized functions has no mathematical meaning (see, e.g., Shilov, 1968), it appears understandable that there is no way to define the Reynolds stress tensor of turbulent motion (section, "Reynolds Stresses and Eddy Dissipation") by a meaningful ordinary or generalized function, because it contains quadratic products of the so-called fluctuating velocity residuals (see, e.g., Schlichting, 1968). However, its energy-dissipating (stresslike) effect is physically quite apparent and must be modeled in some macroscopic sense.

To avoid all conceptual difficulties of microscopic turbulent motions, it seems natural to fall back to the discrete (macroscopic) description of laminar flows that leads formally to the Navier-Stokes equations. In fact, by proper "generalized" interpretation, most motions used in the laminar regime retain their physical meaning in the discrete turbulent domain. For example, the "mean" x -velocity, u , of a "flow parcel" contained in a rectangular test (grid) cell of mesh lengths Δx , Δy , and Δz (Figure 3a) at some time, t , of a time interval, Δt , is defined as the mass flux (ΔM^2) crossing, say the central ($x = x_1$) surface element (Δy , Δz) of the

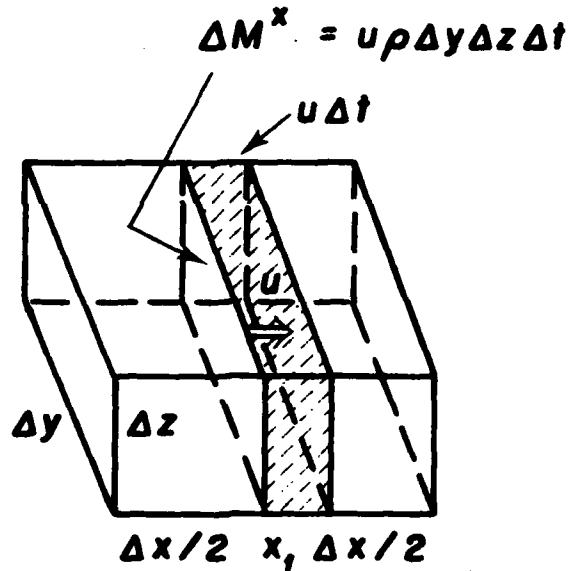


Figure 3a. Illustration of average velocity: ΔM^x = mass flux in x-direction, u = mean velocity in x-direction, and ρ = fluid density.

cell during the time span Δt divided by the fluid density, ρ , the area, $\Delta y \cdot \Delta z$, and the time, Δt , so that

$$u = \Delta M^x / \rho \Delta y \Delta z \Delta t. \quad (111)$$

This (generalized) definition of the mean-flow velocity, u , is uniformly valid for laminar and turbulent motions, since ΔM^x is a physically realistic (measurable) quantity for any $\rho > 0$, $\Delta x > 0$, $\Delta y > 0$, $\Delta z > 0$, and $\Delta t > 0$. If u exists in the limit $\Delta x \rightarrow 0$, $\Delta y \rightarrow 0$, $\Delta z \rightarrow 0$, and $\Delta t \rightarrow 0$, then u becomes the ordinary particle (or point) velocity. This assumption is well justified in most (see above) laminar motions, where neighboring particles flow on smooth neighboring pathlines. In contrast to laminar flow, the limit assumption is certainly not justified in turbulent flow, where the fluid particles move in an indeterministically turbulent, "fluctuating," or

“eddy” way. In the sense of generalized functions, u could be defined in the limit by prescribing its mass flux (ΔM^x) for every nonvanishing ρ , Δx , Δy , Δz , and Δt .

Using similarly generalized definitions of all mean velocity components and pressure, and retaining their finite differences in place of (generally non-existent) ordinary derivatives, one arrives as usual at the discrete Navier–Stokes equations (analog of Equations 1 and 2) without requiring the existence of any limit values (see, e.g., Schlichting, 1968; Whitaker, 1968). They express simply the physical laws of conservation of momentum and mass for every test (mesh) cell. This is particularly tangible for the DOTE (Equation 61), which conserves mass by balancing the excess of mass flux into a mesh cell with a corresponding increment in tidal height.

In the discrete form, the Navier–Stokes equations look formally the same for laminar and turbulent motions. Yet, when in the laminar case velocity and pressure exist pointwise in the limit, one has a unique microscopic (continuous) description of the flow subject only to specified boundary and initial conditions. Hence, the quality of a solution of the discrete model can be measured against the so-called exact integral of the continuous equations. In sharp contrast to the laminar case, no unique microscopic description of turbulent flow exists against which the quality of the discrete model could be measured. Therefore, the numerical analyst must seek an optimum size of the mesh cell (Δx , Δy , Δz) and the time span (Δt) in order to model the undetermined microscopic turbulent motion so that their macroscopic effects match the expected or observed features.

The strong dependence of a discrete turbulent-flow model on the size of the mesh cell (Δx , Δy , Δz) and the time span (Δt) can be assessed, for instance, from the definition of the average velocity, u , by Equation 111. With increasing mesh area ($\Delta y \cdot \Delta z$), more and more as well as larger and larger fluctuating or eddy motions are filtered out and remain unaccounted for in the average value of u . Hence, the maximum mesh lengths Δx , Δy , and Δz must be sufficiently smaller than the smallest wave length one wishes to resolve. On the other side, if the area ($\Delta y \cdot \Delta z$) in Equation 111 is

chosen smaller and smaller, then u becomes more and more undetermined (fluctuating).

Similar arguments determine an optimum time step, Δt . In the present discrete tide model, the cell size was reasonably limited by the available bathymetric tables. The time step Δt (Equation 105) was determined by trial-and-error computations, so that 60 time points represent one-quarter of the M_2 -tide period.

Another significant distinction between the discrete Navier-Stokes equations of laminar and turbulent flow becomes apparent in the average stress tensor. As is well known, the turbulent fluctuations neglected in the mean velocity and pressure manifest themselves as stresslike (energy-dissipating) forces that affect the mean motion. Unfortunately, no exact and unique constitutive equation is known today that relates those turbulent Reynolds stresses to the mean rate of strain (deformation of the flow parcel) determined by the average velocity (see, e.g., Schlichting, 1968; Whitaker, 1968). In the Boussinesq (1877) substitution used in the present tide model, the mean-turbulent-stress tensor is directly related to the average rate of strain (analog of Equations 5). Hence, the macroscopic stress effects of the turbulent fluctuations on the mean velocity are assumed to follow a similar simple law as the viscous laminar stresses in Newtonian fluids. Only the coefficient of viscosity is replaced by the so-called eddy viscosity, which remains to be modeled to account for the otherwise neglected eddying motions in some best sense.

In the absence of better approximations, it seems idle to argue about the physical justification of the Boussinesq substitution; the fact remains that it represents the simplest possible constitutive equation, including zero used by some researchers. Moreover, it provides for considerable flexibility to model the microscopically undetermined but macroscopically apparent eddy dissipation by choosing suitable velocity-dependent or velocity-independent eddy viscosities either uniformly or separately for all three stress directions. Evidently, if the velocity field were known, *a priori*, then one could determine exact eddy viscosities, *a posteriori*, in many ways. In this connection, it is of interest to know that the mean flow is

quite insensitive to fairly large variations (say 25%) of the eddy viscosity. This observation by Munk and Palmén (1951) was confirmed for oceanic tidal motions by the author's extensive computer experiments. It is probably related to the well-known fact that potential motions satisfy the complete Navier-Stokes equations of laminar flow with any constant viscosity. Above all, as with any other physical law, the Boussinesq substitution has successfully passed its crucial test in many practical applications in hydrodynamics, oceanography, and meteorology. The present ocean-tide model is no exception (see Schwideraki, 1979b, 1979c).

In order to illustrate the Boussinesq substitution in the discrete case, one may consider, for example, the average normal stress τ^{xx} produced by the filtered out (see the remarks to Equation 111) fluctuating motions on the surface $(\Delta y, \Delta z)$ at $x = x_1$ shown in Figure 3b. Following Boussinesq, one has (see the analogous Equation 5c)

$$\tau_1^{xx} = 2A\rho \frac{u_2 - u_0}{2\Delta x} \tag{112a}$$

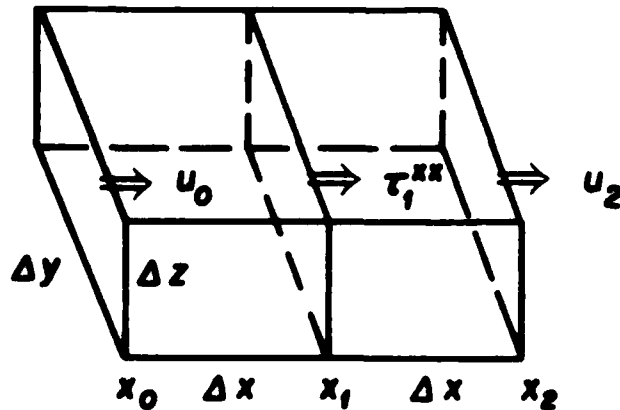


Figure 3b. Illustration of mean normal stress: u_0, u_2 = average x-velocities at $x = x_0, x_2$, and τ_1^{xx} = average normal stress.

where u_0 and u_2 are the corresponding mean velocities at $x = x_0 = x_1 - \Delta x$ and $x = x_2 = x_1 + \Delta x$. Hence, the turbulent stress τ_1^{xx} grows linearly with the rate of change of average velocity. Analogous to the corresponding laminar stress, this linear law appears physically acceptable, since the expected mean tidal velocities are small. One concludes from Equation 112a that a large change of mean flow produces a large turbulent stress, which plausibly must be due to strong fluctuating motions.

If one assumes a constant eddy viscosity, A , in Equation 112a, then the analogy between turbulent and laminar stress becomes complete. However, as was pointed out above, the strength of the fluctuating motions under consideration depends on the size of the surface area ($\Delta y \cdot \Delta z$), which justifies the assumption

$$A = a\Delta y\Delta z \quad (112b)$$

in Equation 112a, where a may be held constant or used for further modeling. Similar arguments can be developed for all six turbulent stress components (see Equations 5) with eddy viscosities equivalent to Equation 112b.

The novel eddy-viscosity law expressed by Equation 112b is obviously equivalent to the eddy viscosity introduced in the present tide model by Equation 6a. It also explains Equation 4a, which specifies the bottom-friction coefficient, B , of the discrete tide model. The need for a mesh-area-dependent eddy viscosity became apparent when initial tidal computations with a constant value failed to yield realistic results. It must be emphasized that the microscopically indeterministic nature of turbulent motions is not completely removed in the discrete flow model. Its specific macroscopic effects on the mean flow are apparent in the required optimum choice of the grid system, time step, differencing parameters, and most of all, the eddy-viscosity law and scaling coefficient. No information on the fine structure of the turbulence can be expected from such a model.

Preliminary M_2 -Tide Results

The fully specified tidal equations (DOTEs 60, 61) have been applied to construct the principal semidiurnal lunar ocean tide (M_2). The results (Schwiderski, 1976) represented a considerable improvement over earlier models. Indeed, they demonstrated the feasibility to achieve the extraordinary accuracy of 10 cm required in many applications. For example, Goad and Douglas (1977a, b), who used the preliminary model to determine the M_2 -tide effects on the moon's orbital parameters, found satisfactory agreement with other theories and observations.

Due to the absence of an exact continuous ocean-tide model (preceding section), the degree of reality achieved by any approximate discrete model must be measured against empirically known features of ocean tides. Fortunately, for the M_2 ocean tide a large number (e.g., British Admiralty Tide Tables, 1977) of tidal observations around the world oceans are available for comparison. Table 2 gives a statistical evaluation of the computed preliminary M_2 -tide in comparison to observations made at 20 island tide-gauge stations in each of the Atlantic, Indian, and Pacific oceans. The agreements found are encouraging.

Table 2
Comparison of preliminary M_2 ocean tide model with empirical data.

Ocean	Number of Islands	Amplitude Differences		Phase Differences	
		Mean	RMS	Mean	RMS
Atlantic	20	-0.6 cm	10.9 cm	8.8°	14.4°
Indian	20	+1.9 cm	15.1 cm	5.5°	19.7°
Pacific	20	+7.4 cm	12.9 cm	2.8°	17.4°

While the preliminary M_2 ocean tide model displayed good agreement with most tidal observations over large ocean areas, significant shortcomings still persisted, especially over narrow ocean ridges such as the Aleutian, Hawaiian, Marianas, and Caribbean ridges. By comparing tidal observations on both sides of such ridges

experimental tidalists (see, e.g., Harris, 1904; Bogdanov, 1961; Defant, 1961; Luther and Wunsch, 1975) very early discovered drastic distortion and retardation effects of those bottom barriers on ocean tides (see the tables in Part II of this paper, Schwiderski, 1979b).

In order to model local tide distortions, the described tide program will be modified in Part II by using a new "hydrodynamically defined ocean bathymetry" that reflects the barrier effects of narrow ridges and other large irregularities of the ocean basin (Schwiderski, 1978a). Moreover, a novel "hydrodynamical interpolation technique" will be introduced to incorporate directly over 2,000 empirical tide data into the construction of the tidal charts. The high numerical quality of the final M_2 ocean tide model will be displayed by maplike tables.

A résumé of this paper was presented at the International Symposium on Interaction of Marine Geodesy and Ocean Dynamics, held from October 10 to 13, 1978, at the Rosenstiel School of Marine and Atmospheric Science, Miami, Florida.

References

- Bogdanov, C. T., 1961, New Charts of the Cotidal Lines of Semidiurnal Tidal Waves (M_2 and S_2) for the Pacific Ocean. Soviet Oceanography, I, p. 28.
- Boussinesq, J., 1877, Théorie de L'écoulement Tourbillant. Mém. Prés. Acad. Sci. XXIII, 46, Paris.
- British Admiralty Tide Tables, 1977, Vols. 1, 2, and 3.
- Busse, F. H., and Whitehead, J. A., 1971, Instabilities of Convection Rolls in a High Prandtl Number Fluid. Journal of Fluid Mechanics, 47, p. 305.
- Cartwright, D. E., and Tayler, R. J., 1971, New Computations of the Tide-Generating Potential. Geophys. J. Roy. Astr. Soc., 23, p. 45.
- Cox, M. D., 1970, A Mathematical Model of the Indian Ocean. Deep-Sea Research, 17, p. 45.
- Darwin, G. H., 1883, Report on the Harmonic Analysis of Tidal Observations. Brit. Assoc. for Adv. Sci. Rep., See also Sci. Pap. 1, Cambridge, 1907.

- Defant, A., 1961, *Physical Oceanography*. New York: Pergamon Press, Vol. II.
- Dietrich, G., 1963, *General Oceanography*. New York: Interscience Publishers, John Wiley & Sons.
- Doodson, A. T., 1921, The Harmonic Development of the Tide-Generating Potential. Proc. Roy. Soc., London, Ser. A, 100.
- Estes, R., 1975, A Computer Software System for the Generation of Global Numerical Solutions of Diurnal and Semidiurnal Ocean Tides. Contract NAS5-20045, Business and Technol. Syst. TR-75-27.
- Estes, R., 1977, A Computer Software System for the Generation of Global Ocean Tides Including Crustal Loading Effects. Contract NAS5-20045, Business and Technol. Syst. TR-77-41.
- Farrell, W. E., 1972a, Deformation of the Earth by Surface Loads. Rev. Geophys. Space Phys., 10, p. 261.
- Farrell, W. E., 1972b, Global Calculations of Tidal Loading. Nature, 238, p. 43.
- Farrell, W. E., 1973, Earth Tides, Ocean Tides, and Tidal Loading. Phil. Trans. Roy. Soc., London, Ser. A, 274, p. 253.
- Friedrich, H. J., 1970, Preliminary Results from a Numerical Multi-layer Model for the Circulation in the North Atlantic. Deutsche Hydr. Zeit., 23, p. 145.
- Goad, C. C., and Douglas, B. C., 1977a, Determination of the M_2 Ocean Tide Parameters from Satellite Orbit Perturbations. J. Geophys. Res., 82, p. 898.
- Goad, C. C., and Douglas, B. C., 1977b, Lunar Longitude Deceleration and Tidal Parameters Estimated from Satellite Orbital Perturbations. Presented to the Eighth International Symposium on Earth Tides, Bonn, Federal Republic of Germany.
- Grace, S. F., 1931, The Semi-diurnal Lunar Tidal Motion of the Red Sea. Mon. Not. Roy. Astr. Soc., Geophys. Suppl. 2, p. 316.
- Hansen, W., 1966, Die Reproduktion der Bewegungsvorgänge im Meere mit Hilfe Hydrodynamisch-Numerischer Verfahren. Mitteilungen des Inst. f. Meereskunde der Univ. Hamburg, V.
- Harris, R. A., 1904, Manual of Tides, Part IVb. Report of the Superintendent, U.S. Coast and Geodetic Survey, p. 313.
- Hendershott, M. C., 1972, The Effects of Solid-Earth Deformation on Global Ocean Tides. Geophys. J. Roy. Astr. Soc., 29, p. 380.
- Hendershott, M. C., 1975, Global Numerical Tide Solutions with In-

- clusion of Ocean Self-Gravitation and of Solid Earth Tidal Loading. XVI General Assembly of IUGG, Grenoble, France.
- Hendershott, M. C., 1977, Numerical Models of Ocean Tides. *The Sea*, Vol. 6, p. 47.
- Holland, W. R., and Hirschman, A. D., 1972, A Numerical Calculation of the Circulation in the North Atlantic Ocean. *J. Phys. Oceanogr.* 2, p. 336.
- Ladyzhenskaya, O. A., 1969, *The Mathematical Theory of Viscous Incompressible Flow*. New York: Science Publishers, Gordon and Breach.
- Luther, D. S., and Wunsch, C., 1975, Tidal Charts of the Central Pacific Ocean. *J. Phys. Ocean.*, 5, p. 227.
- Munk, W. H., and Palmen, E., 1951, Note on the Dynamics of the Antarctic Circumpolar Current. *Tellus*, 3, p. 53.
- Pekeris, C. L., and Accad, Y., 1969, Solution of Laplace's Equation for the M_2 Tide in the World Oceans. *Phil. Trans. Roy. Soc., London*, Ser. A, 265, p. 413.
- Richardson, L. F., 1922, *Weather Prediction by Numerical Methods*. London: Cambridge University Press.
- Richtmyer, R. D., 1957, *Difference Methods for Initial-Value Problems*. New York: Interscience Publishers, Inc.
- Schlichting, H., 1968, *Boundary-Layer Theory*. New York: McGraw-Hill Book Co.
- Schwiderski, E. W., 1972, Bifurcation of Convection in Internally Heated Fluid Layers. *The Phys. of Fluids*, 15, p. 1882.
- Schwiderski, E. W., 1976, Preliminary M_2 Tide. Computer Tape, NSWC/DL, Dahlgren, Virginia.
- Schwiderski, E. W., 1978a, Hydrodynamically Defined Ocean Bathymetry. NSWC/DL-TR 3888.
- Schwiderski, E. W., 1978b, Global Ocean Tides, Part I: A Detailed Hydrodynamical Interpolation Model. NSWC/DL-TR 3866.
- Schwiderski, E. W., 1979a, On Charting Global Ocean Tides. Review Paper in preparation.
- Schwiderski, E. W., 1979b, Ocean Tides, Part II: A Hydrodynamical Interpolation Model. *Marine Geodesy*, Vol. 3.
- Schwiderski, E. W., 1979c, Global Ocean Tides, Part II: The Semi-diurnal Principal Lunar Tide (M_2). NSWC/DL-TR (in press).
- Shilov, G. E., 1968, *Generalized Functions and Partial Differential Equations*. New York: Gordon and Breach.

- Smith, S. M., Menard, H. M., and Sharman, G., 1966, World-wide Ocean Depths and Continental Elevations Averaged for Areas Approximating One-Degree Squares of Latitude and Longitude. Ref. 65-8, Scripps Institution of Oceanography, LaJolla, California.
- Thomson, W. (Lord Kelvin), 1868, Report of Committee for the Purpose of Harmonic Analysis of Tidal Observations. Brit. Assoc. Adv. Sci. Rep., London.
- Whitaker, S., 1968, *Introduction to Fluid Mechanics*. Englewood Cliffs, New Jersey: Prentice-Hall, Inc.
- Zahel, W., 1970, Die Reproduktion Gezeitenbedingter Bewegungsvorgänge im Weltozean Mittels des Hydrodynamisch-Numerischen Verfahrens. Mitteilungen des Inst. f. Meereskunde der Univ. Hamburg, XVII.
- Zahel, W., 1973, The Diurnal K_1 Tide in the World Ocean—A Numerical Investigation. *Pure Appl. Geophys.*, 109, p. 1819.
- Zahel, W., 1975, A Global Hydrodynamic-Numerical 1° Model of the Ocean Tides. The Oscillation System of the M_2 Tide and Its Distribution of Energy Dissipation. XVI General Assembly of IUGG, Grenoble, France.